

What Controls the Mean East–West Sea Surface Temperature Gradient in the Equatorial Pacific: The Role of Cloud Albedo

N. J. BURLS AND A. V. FEDOROV

Department of Geology and Geophysics, Yale University, New Haven, Connecticut

(Manuscript received 22 April 2013, in final form 3 January 2014)

ABSTRACT

The mean east–west sea surface temperature gradient along the equator is a key feature of tropical climate. Tightly coupled to the atmospheric Walker circulation and the oceanic east–west thermocline tilt, it effectively defines tropical climate conditions. In the Pacific, its presence permits the El Niño–Southern Oscillation phenomenon. What determines this temperature gradient within the fully coupled ocean–atmosphere system is therefore a central question in climate dynamics, critical for understanding past and future climates. Using a comprehensive coupled model [Community Earth System Model (CESM)], the authors demonstrate how the meridional gradient in cloud albedo between the tropics and midlatitudes ($\Delta\alpha$) sets the mean east–west sea surface temperature gradient in the equatorial Pacific. To change $\Delta\alpha$ in the numerical experiments, the authors change the optical properties of clouds by modifying the atmospheric water path, but only in the shortwave radiation scheme of the model. When $\Delta\alpha$ is varied from approximately -0.15 to 0.1 , the east–west SST contrast in the equatorial Pacific reduces from 7.5°C to less than 1°C and the Walker circulation nearly collapses. These experiments reveal a near-linear dependence between $\Delta\alpha$ and the zonal temperature gradient, which generally agrees with results from the Coupled Model Intercomparison Project phase 5 (CMIP5) preindustrial control simulations. The authors explain the close relation between the two variables using an energy balance model incorporating the essential dynamics of the warm pool, cold tongue, and Walker circulation complex.

1. Introduction

A salient feature of present-day climate is the pronounced east–west gradient in equatorial Pacific sea surface temperature (SST). In the equatorial band between 3°S and 3°N , surface temperatures range from approximately 29°C in the western warm pool to 23°C in the eastern cold tongue region. A similar, albeit weaker, temperature contrast exists in the Atlantic Ocean as well. These zonal SST gradients are coupled to atmospheric zonal circulation, referred to as the Walker cells (Bjerknes 1969), that control the zonal tilt of the oceanic thermocline and the strength of equatorial upwelling. Paleoclimate records suggest, however, that the mean state of the equatorial Pacific has not always been characterized by such sharp zonal SST gradients. In particular, paleodata suggest weak zonal temperature gradients, perhaps below 1° – 2°C , during some of the warm periods in Earth's history, such as the early Pliocene (Wara

et al. 2005; Fedorov et al. 2006; Ravelo et al. 2006; Dekens et al. 2008; Fedorov et al. 2013). In the more recent past, the mid-Holocene, there is evidence of a gradient slightly stronger than today (Koutavas et al. 2006). At the same time, state-of-the-art global climate models (GCMs) simulate different values of this gradient for the modern climate (see section 5) and yield conflicting projections for its changes with global warming (Collins 2005; DiNezio et al. 2009). Thus, paleoevidence and results from climate models prompt the fundamental question: what sets the mean east–west gradient in equatorial Pacific SST?

The first, tentative answers to this question depend on which component of the coupled ocean–atmosphere system we choose to focus on. From an oceanic perspective, the presence of a sharp, shallow equatorial thermocline that shoals from west to east together with the strong wind-driven equatorial upwelling are critical for maintaining the mean SST gradient. It is the strength of the wind-driven shallow subtropical cells (STCs) (McCreary and Lu 1994) and the temperature of the water subducted into these cells in the extratropics (Gu and Philander 1997; Boccaletti et al. 2004) that determine the temperature of water upwelled in the eastern equatorial

Corresponding author address: N. J. Burls, Department of Geology and Geophysics, Yale University, P.O. Box 208109, New Haven, CT 06520-8109.
E-mail: natalie.burls@yale.edu

Pacific. Local processes that influence the strength of the surface heat flux further modify the eastern Pacific SST (Ma et al. 1996; Wang and McPhaden 1999). In the western Pacific, where mean equatorial trade winds maintain a deeper thermocline, SST is largely controlled by local radiative forcing; nevertheless, the role of wind-driven ocean dynamics cannot be overlooked when considering the maintenance of the climatological mean state (Sun and Liu 1996; Clement et al. 2005).

From an atmospheric perspective, however, it is the global SST structure that controls surface winds, directly (in the equatorial region) or indirectly (in the extratropics), thus determining wind-driven subduction and upwelling. Along the equator, the zonal SST gradient and Walker circulation are tightly coupled (Bjerknes 1969). A close relationship also exists between the meridional SST gradient and the strength of the Hadley circulation (McWilliams and Gent 1978; Liu and Huang 1997)—more exactly, it is the meridional gradient in subcloud-layer equivalent potential temperature (Emanuel et al. 1994) that controls the strength of the Hadley cells, but these two gradients are in general closely related. Thus, when we turn to the atmosphere to establish the mechanisms dictating SST, we are confronted with a circular argument.

Consequently, the question of the east–west SST gradient in the equatorial Pacific should be addressed from the fully coupled ocean–atmosphere perspective. McWilliams and Gent (1978), Dijkstra and Neelin (1995), and Liu and Huang (1997) have all presented coupled theories addressing the mechanism that determines the strength of the climatological warm pool, cold tongue, Walker circulation complex (WCWC). The theory of Liu and Huang (1997) is the most complete in that it encompasses the extratropics and thereby the influence that the tropical and extratropical oceans have on one another via the shallow meridional overturning circulation of the STCs. As discussed in more detail in section 5, a key aspect of the coupled system evident in the analytical results of Liu and Huang is that in the steady state the WCWC is regulated by a kinematic constraint: a saturation east–west SST difference of approximately one-quarter the meridional gradient in local-equilibrium SST (the temperature gradient that the ocean would have in the absence of oceanic heat transport) can be reached for a modest coupling strength between equatorial SST, trade winds, and ocean transport. Liu and Huang (1997) suggest that the Pacific today has reached this saturation state, so the mean east–west SST gradient is primarily determined by the meridional gradient in the temperature toward which the ocean surface is being restored by the overlying atmosphere.

An implied feature of this theory is that, as the mean east–west SST gradient increases, so too must the mean surface heat flux into the tropical Pacific Ocean, and hence the poleward ocean heat transport out of the tropical Pacific—in the steady state the net ocean heat transport from the tropical Pacific must balance the net surface heat gain in the tropical Pacific and surface heat loss in the extratropical Pacific under the constraint of a balanced heat budget (Boccaletti et al. 2004). For example, in a world where the mean east–west SST gradient has decreased, the poleward ocean heat transport must also decrease.

In light of the above argument one can consider past climates that maintained a SST gradient quite different from today. For example, despite a similar continental configuration, proxy data indicates that the east–west gradient was substantially weaker in the tropical Pacific during the early Pliocene (Wara et al. 2005; Fedorov et al. 2006; Ravelo et al. 2006; Fedorov et al. 2013). The physical processes that maintained the tropical Pacific climate of the early Pliocene (4–5 million years ago) remain unclear. Simulations of the mid-Pliocene conducted using GCMs forced with reconstructed boundary conditions [CO_2 at 400 ppm and Pliocene Research, Interpretation, and Synoptic Mapping (PRISM) reconstructed surface boundary conditions] fail to fully reproduce the reduced gradient condition suggested by paleoclimatic evidence (Haywood et al. 2007; Lunt et al. 2010; Dowsett et al. 2012). Purely increasing CO_2 or modifying oceanic gateways does not achieve, within a state-of-the-art GCM, the structurally different tropical climate revealed by paleoclimate data (Fedorov et al. 2013).

The reason why GCMs fail becomes apparent when one considers the implied poleward heat transport demanded by either the atmospheric or the oceanic component from the other component when run in isolation (Brierley et al. 2009). An atmospheric general circulation model forced with reconstructed early Pliocene SSTs implies that the heat transport by the ocean was greater than today (Barreiro et al. 2006; Brierley et al. 2009). However, the theory mentioned above and the results obtained based on ocean general circulation models with low vertical diffusion suggest that a weaker zonal SST gradient is associated with reduced oceanic heat transport (Philander and Fedorov 2003) as the net surface heat flux into the equatorial ocean is reduced. The missing mechanism therefore appears to lie in identifying a process, currently unresolved by GCMs, that would have acted within the warm world of the Pliocene to decrease the required ocean heat transport out of the tropical Pacific.

Such a reduction in ocean poleward heat transport can be achieved by two principally different means. The first

is a change in the partitioning of heat transport between the ocean and the atmosphere, while keeping the total heat transport approximately constant. It has been suggested that increased vertical mixing of the upper ocean by hurricanes could do just that, and hence could be a missing mechanism (Fedorov et al. 2010). By allowing the ocean to gain heat over a larger area, hurricanes could have driven increased heat uptake off the equator, thereby reducing the required oceanic heat uptake within the equatorial band. This mechanism amounts to changing the partitioning of the poleward heat transport between the tropical ocean and atmosphere.

The second possible scenario for decreasing ocean heat transport is a reduction of the total poleward heat transport of the system. Such a climate would support a structurally different radiation budget at the top of the atmosphere relative to today—a radiation budget where the total poleward heat transport required by both oceanic and atmospheric components of the coupled system is reduced and outgoing radiation balanced more locally by incoming radiation. The present study focuses on this particular scenario. As demonstrated by Donohoe and Battisti (2012), the spread in meridional heat transport within Coupled Model Intercomparison Project (CMIP) GCMs is primarily due to their spread in cloud reflection properties. A mechanism put forward for the early Pliocene is reduced low-level cloud formation in the extratropics (Barreiro and Philander 2008). Such a change would act to decrease extratropical cloud albedo, increase the amount of solar radiation absorbed by the ocean in the higher latitudes, increase the temperature of water subducted within the STCs, decrease the static stability of the ocean, inhibit the surfacing of colder deep water in the tropics, and maintain a weak zonal SST gradient.

Barreiro and Philander (2008) conducted several numerical experiments that generally supported this mechanism using a coupled climate model consisting of a simplified atmospheric model. However, in their model the reduction of the east–west gradient was relatively modest, on the order of 1°C, even for a 50% reduction in low-cloud cover in the extratropics. Consequently, several key questions remained unresolved: Is cloud albedo indeed a critical factor that controls the east–west SST gradient? Which patterns of cloud albedo change are especially effective in modifying this gradient? What is the spatial extent and magnitude of the cloud albedo changes required to reduce this gradient to Pliocene-like values?

In the present study we systematically explore, under a wide range of climates, the robustness of our theoretical understanding of what controls the mean east–west SST gradient in equatorial Pacific using spatial

variations in cloud albedo as a means to modify the meridional gradient in local-equilibrium SST, as well as the required poleward ocean heat transport. As elaborated on in the following section, we employ a state-of-the-art, fully coupled climate model to simulate and analyze the response of the coupled system to changes in the albedo of extratropical as well as tropical clouds. While the changes in cloud albedo imposed are purely hypothetical, possible causes could, for example, be changes in atmospheric aerosol concentrations (Kiehl and Shields 2014; Kump and Pollard 2008), which can be imposed independent of the leading-order coupled system dynamics. As the central result of this study we demonstrate that the mean east–west SST gradient depends almost linearly on the meridional albedo gradient.

2. Experimental setup: Modifying cloud albedo

The coupled climate model employed within this study is the National Center for Atmospheric Research (NCAR) Community Earth System Model (CESM), version 1.0.4. Simulations have been performed using both a low-resolution and a high-resolution configuration. For the low-resolution configuration (CESM T31 gx3v7), the atmospheric component has a spectral truncation of T31, and the oceanic component has a resolution varying from about 3° near the poles to 1° at the equator. For the high-resolution configuration (CESM 0.9 × 1.25 gx1v6), the atmospheric and oceanic components both have a resolution of about 1°. We will refer to these configurations as T31 and 1° respectively. A description and validation of previous versions of the T31 and 1° configurations (Community Climate System Model, version 4) are provided by Shields et al. (2012) and Gent et al. (2011). The majority of our experiments have been conducted using the T31 configuration as it is computationally cheap relative to the 1° configuration. The 1° experiments serve to assess how robust the T31 results are when the dynamics are better resolved. Atmospheric conditions are set to preindustrial and modern continental geometry is used.

In the modified cloud optics experiments conducted we have systematically changed the optical properties of clouds by modifying the atmospheric liquid water path (LWP) either in just the extratropics or in both the extratropics and the tropics (Fig. 1), but only in the shortwave radiation scheme. These modifications effectively change the albedo of highly reflective low stratus clouds when they form in the model. When making changes in the tropical band, we also modify the atmospheric ice path (IP), thereby also affecting the albedo of high clouds. The liquid water and ice paths remain unaltered in the longwave radiation scheme. The experiments undertaken fall

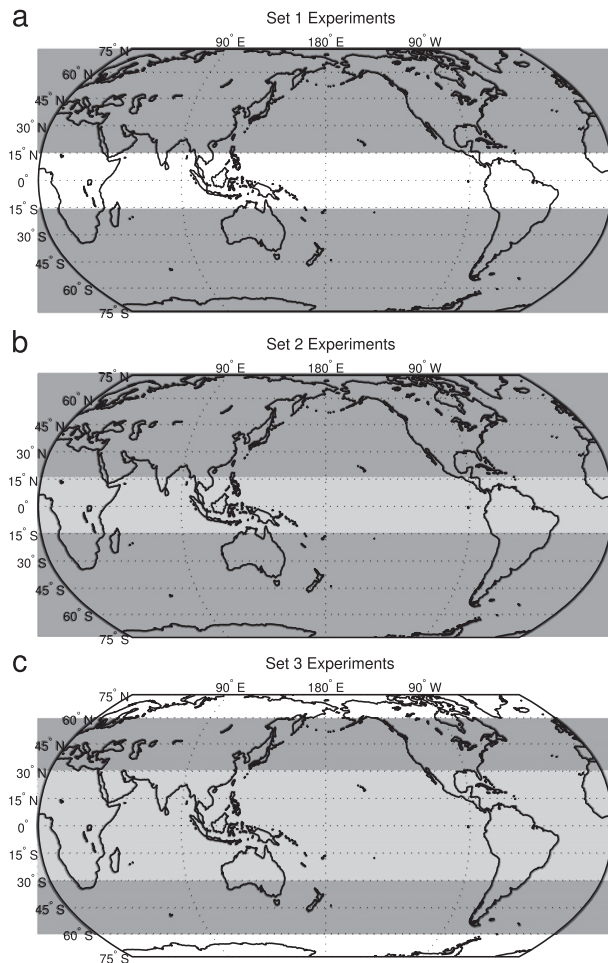


FIG. 1. The regional extent of the imposed modifications in atmospheric water path. Dark (light) shading indicates the regions over which cloud albedo has been systematically reduced (increased) for the experiments of (a) set 1, (b) set 2, and (c) set 3.

into four main sets. Table 1 specifies the modifications in water path imposed within each of the four sets of experiments and the resulting tropical (8°S – 8°N) and extratropical (8° – 65°N/S) Pacific albedo changes. For the purposes of this sensitivity study, modifying the atmospheric water path serves as an efficient and relatively straightforward way of imposing cloud albedo changes within a comprehensive GCM. The cloud albedo changes resulting from our imposed water path changes could, however, be realized by changes in a number of cloud properties in addition to liquid and ice water content, for example, cloud lifetime and particle concentration and size. While Table 1 has been included in the manuscript for transparency, we are not suggesting that atmospheric water path changes are necessarily the sole mechanism maintaining the changes in albedo required to support, for example, the weak gradients of the early Pliocene.

These sensitivity experiments are designed to consider a change in the cloud radiative forcing associated with low-level clouds. Having a large shortwave forcing but little longwave forcing these clouds can induce a change in the net top-of-atmosphere (TOA) radiation balance and a cloud feedback (Stephens and Greenwald 1991; Hartmann et al. 1992; Stephens 2005). In the tropics, however, we impose a change in the shortwave forcing of both low and high clouds by changing both the liquid and ice path. Unlike low clouds, high clouds within the tropics have a strong longwave forcing that largely offsets the shortwave forcing, resulting in near TOA cancellation between the longwave and shortwave cloud forcing (Stephens and Greenwald 1991; Kiehl 1994; Stephens 2005). Significant interannual variability is, however, observed in the extent of this TOA cancellation owing to changes in tropical circulation patterns (e.g., shortwave cooling dominated during the 1998 El Niño event) (Cess et al. 2001; Allan et al. 2002). Moreover, Hartmann and Larson (2002) suggest that the emission temperature of tropical convective clouds should remain constant during climate change. By only perturbing the shortwave forcing associated with tropical clouds, we allow the system to freely adjust its longwave forcing.

Considerable interannual and decadal variability is observed in cloud radiative forcing due to volcanic eruptions, El Niño events, and large-scale changes in Hadley and Walker strength (Wielicki et al. 2002; Chen et al. 2002; Allan et al. 2002). This variability is poorly captured by climate models (Wielicki et al. 2002; Cess et al. 2001; Allan et al. 2002). Our understanding of changes in cloud radiative forcing within paleoclimates is even more uncertain. A recent study by Kiehl and Shields (2014), exploring the general sensitivity of the Paleocene–Eocene Thermal Maximum climate state to changes in cloud microphysical properties, assumes that all cloud condensation nuclei (CCN) values were closer to those observed in present day pristine conditions. While the associated change in cloud albedo is not explicitly mentioned, the CCN-induced changes in cloud properties yield a 7° to 9°C warming at the poles, comparable to the extremes of our experimental range. Kump and Pollard (2008) suggest that reduced CCN during the warm equable climate of the Cretaceous could have supported less extensive and optically thinner clouds, reducing planetary albedo from 0.30 to 0.24. This reduction in cloud albedo is required in addition to elevated CO_2 levels to produce the extreme high-latitude warmth implied by proxy data for the middle Cretaceous (Kump and Pollard 2008).

Within this sensitivity study we have imposed a range of changes to the cloud forcing. The first three sets

TABLE 1. CESM experiments conducted.

Expt	Cloud water path modification	Tropical Pacific Albedo change	Extratropical Pacific Albedo change
1	T31 Control—No cloud water path modification		
	Set 1		
2	15°–90°N/S LWP increased by 80% and unmodified elsewhere	–0.016	0.031
3	15°–90°N/S LWP increased by 60% and unmodified elsewhere	–0.010	0.022
4	15°–90°N/S LWP increased by 40% and unmodified elsewhere	–0.007	0.016
5	15°–90°N/S LWP increased by 20% and unmodified elsewhere	–0.005	0.008
6	15°–90°N/S LWP reduced by 20% and unmodified elsewhere	0.009	–0.010
7	15°–90°N/S LWP reduced by 40% and unmodified elsewhere	0.018	–0.025
8	15°–90°N/S LWP reduced by 60% and unmodified elsewhere	0.031	–0.045
9	15°–90°N/S LWP reduced by 80% and unmodified elsewhere	0.056	–0.072
	Set 2		
10	15°–90°N/S LWP reduced by 20% and 15°S–15°N IP and LWP increased by 40%	0.016	–0.008
11	15°–90°N/S LWP reduced by 40% and 15°S–15°N IP and LWP increased by 80%	0.038	–0.022
12	15°–90°N/S LWP reduced by 60% and 15°S–15°N IP and LWP increased by 120%	0.062	–0.040
13	15°–90°N/S LWP reduced by 80% and 15°S–15°N IP and LWP increased by 160%	0.086	–0.068
14	15°–90°N/S LWP reduced by 20% and 15°S–15°N IP and LWP increased by 80%	0.024	–0.008
15	15°–90°N/S LWP reduced by 40% and 15°S–15°N IP and LWP increased by 160%	0.047	–0.021
16	15°–90°N/S LWP reduced by 60% and 15°S–15°N IP and LWP increased by 240%	0.073	–0.039
17	15°–90°N/S LWP reduced by 80% and 15°S–15°N IP and LWP increased by 320%	0.104	–0.065
	Set 3		
18	30°–60°N/S LWP reduced by 20% and 30°S–30°N IP and LWP increased by 160%	0.029	0.006
19	30°–60°N/S LWP reduced by 40% and 30°S–30°N IP and LWP increased by 320%	0.049	–0.004
20	30°–60°N/S LWP reduced by 60% and 30°S–30°N IP and LWP increased by 480%	0.069	–0.012
21	30°–60°N/S LWP reduced by 80% and 30°S–30°N IP and LWP increased by 640%	0.092	–0.027
22	1°Control—No cloud water path modification		
	Set 4		
23	15°–90°N/S LWP reduced by 40% and unmodified elsewhere	0.004	–0.030
24	15°–90°N/S LWP reduced by 60% and unmodified elsewhere	0.006	–0.050
25	15°–90°N/S LWP reduced by 40% and 15°S–15°N IP and LWP increased by 80%	0.030	–0.033
26	15°–90°N/S LWP reduced by 60% and 15°S–15°N IP and LWP increased by 120%	0.037	–0.043

differ in the extent and location of the regions where the atmospheric water path, and hence local albedo, are modified. Different choices of these regions (Fig. 1) allow us to vary the meridional albedo contrast together with planetary albedo. The fourth set uses the 1° configuration rather than T31.

- 1) Set 1 (experiments 2–9). Only extratropical, low-level cloud albedo is changed by systematically modifying the LWP of clouds formed poleward of 15°S and 15°N (Fig. 1a). This set of experiments is designed to establish how changes in extratropical cloud albedo affect the mean zonal SST gradient in the Pacific and the associated mean state characteristics of the coupled ocean–atmosphere system in the tropics.
- 2) Set 2 (experiments 10–17). Extratropical albedo is decreased as in experiments 6–9 of set 1. However, instead of leaving the tropical band unchanged, we impose a water path modification of the opposite sign in the tropical band between 15°S and 15°N to amplify the unforced tropical compensation in albedo evident in the set 1 experiments (Fig. 1b); for more details, see section 3. For experiments 10–13 we impose a tropical LWP and IP modification that is two times the LWP modification imposed in the extratropics, whereas for experiments 14–17 we impose a tropical modification that is four times that imposed in the extratropics.
- 3) Set 3 (experiments 18–21). In the set 2 experiments, the resulting decrease in extratropical albedo outweighs the increase in tropical albedo such that the global albedo of the planet decreases. Set 3 is designed to achieve a minimal change in global albedo relative to the T31 control simulation. The LWP of clouds formed between 30° and 60°S/N is systematically reduced with a large opposing tropical as well as subtropical (30°S–30°N) albedo modification (Fig. 1c).
- 4) Set 4 (experiments 23–26). This set of experiments repeats some of the previous experiments using the 1°

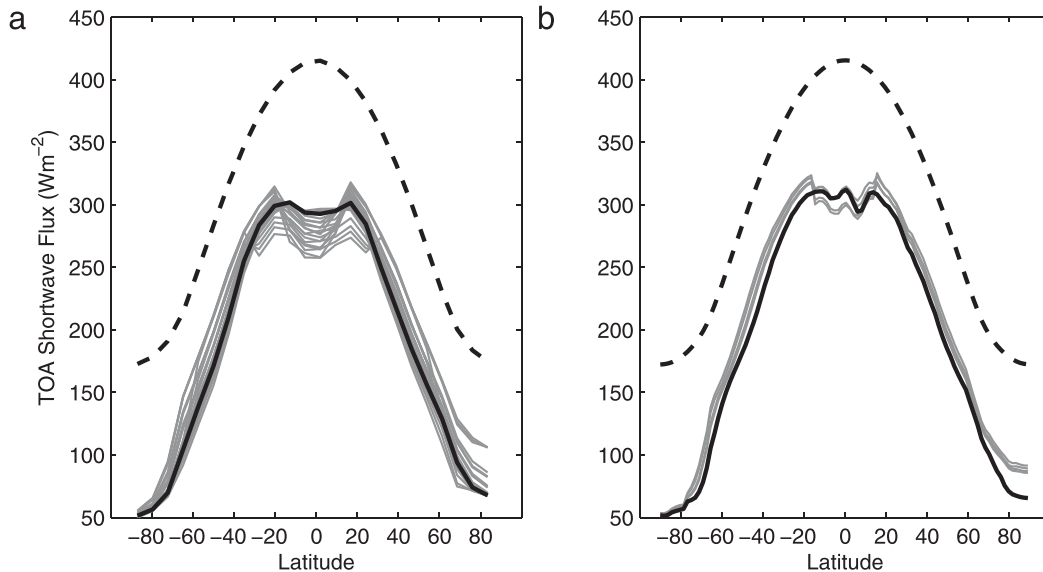


FIG. 2. Shortwave radiation fluxes as a function of latitude in (a) CESM T31 experiments and (b) CESM 1° experiments. The thick dashed black line shows the TOA incoming shortwave radiation for the preindustrial control simulation. The thick solid black line shows the net (incoming minus reflected) TOA shortwave flux for the same preindustrial control simulation, while light gray lines indicate the spread in this variable among different experiments. When the gray lines fall above (beneath) the solid black line, more (less) shortwave radiation reaches the surface relative to the control. The fluxes are zonally averaged.

configuration where the dynamics are better resolved. The goal of these experiments to assess how robust results based on the T31 configuration are.

To allow for the slow adjustment of the deep ocean, all T31 simulations have been run for 800 years. The more computationally demanding 1° configuration experiments have been run for only 200 years—although the deep ocean is still adjusting, by this time the main changes in the shallow tropical and subtropical oceanic circulation that affect SSTs have already occurred. For the T31 configurations we base the analysis on the last 100 years of each simulation, whereas for the 1° configuration we use the last 50 years.

Figures 2 and 3 illustrate the resulting changes in the TOA net shortwave radiative flux. For all T31 experiments performed, Fig. 2a shows the spread in the shortwave forcing resulting from the water path modifications imposed, while Fig. 2b illustrates the change within the 1° experiments. Figure 3 focuses in on the resulting TOA net shortwave radiation changes within the individual experimental sets relative to the control (experiments 1 and 22 are the respective T31 and 1° preindustrial control simulations).

In section 5 the results based on our CESM simulations are compared with observations as well as results from the Coupled Model Intercomparison Project phase 5 (CMIP5) for preindustrial climate conditions

[<http://cmip-pcmdi.llnl.gov>, see Taylor et al. (2012) and Table 2 for all CMIP models]. We use the observed SST data from the NOAA optimum interpolation sea surface temperature (OISST) dataset (Reynolds et al. 2002) and the observed upper-ocean temperature gradients from the climatological *World Ocean Atlas 2009* (WOA2009) dataset (Locarnini et al. 2010). The observed meridional albedo gradient is based on the Clouds and Earth's Radiant Energy System–Energy Balanced and Filled (CERES-EBAF) Ed2.6r data product (Loeb et al. 2009; Wielicki et al. 1996). These data were obtained from the National Aeronautics and Space Administration Langley Research Center Atmospheric Science Data Center (http://ceres.larc.nasa.gov/cmip5_data.php).

Our imposed extratropical (8° – 65° N/S) Pacific albedo modifications range from 0.22 to 0.34, while tropical (8° S– 8° N) Pacific albedo is varied from 0.24 to 0.37. To put our imposed albedo changes into context, mean extratropical Pacific albedo ranges from 0.27 to 0.33, and tropical albedo from 0.19 to 0.29, across the preindustrial CMIP5 models. We can also contrast this against monthly mean albedo values derived from the CERES-EBAF data extending between March 2000 and June 2012. Values range between 0.28 to 0.32 for the extratropical and 0.19 to 0.26 for the tropical Pacific. Our imposed albedo values fall somewhat close to the simulated and observed range for the extratropical Pacific. The

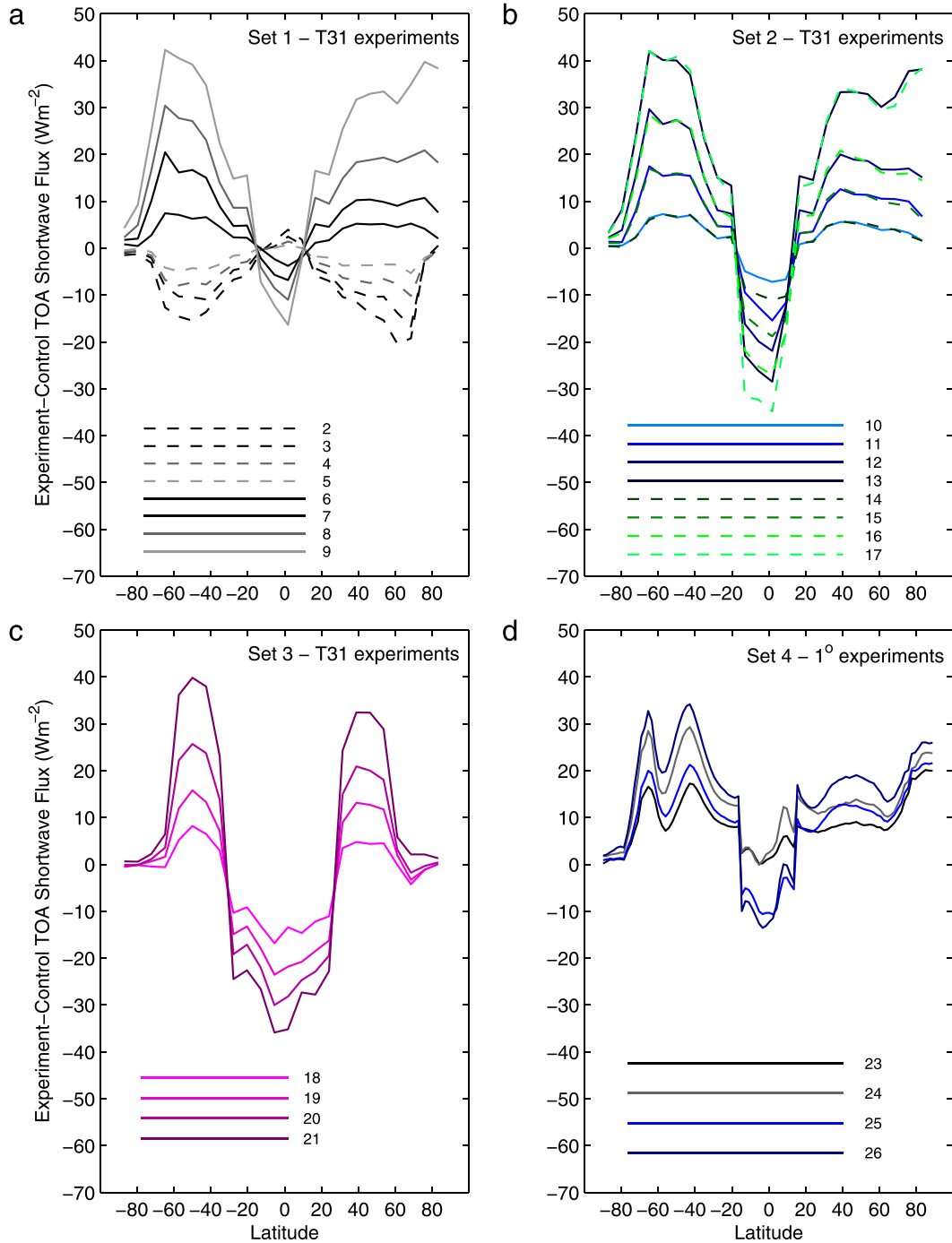


FIG. 3. The difference between each experiment and the control in the zonally averaged net (incoming minus reflected) TOA shortwave flux. (a) Set 1: Only extratropical cloud albedo is modified. (b) Set 2: Extratropical cloud albedo is reduced and an opposing water path modification is applied in the tropics. (c) Set 3: Experiments are designed to achieve a minimal change in global albedo relative to the T31 control simulation. (d) Set 4: The same water path modifications as applied in T31 experiments 7 and 8 (from set 1) and 12 and 13 (from set 2) have been repeated using the 1°CESM configuration (Table 1). The same coloring is used as for the T31 experiment with the corresponding atmospheric path modification.

TABLE 2. CMIP5 models used in this study.

Model and institution	Model acronym
Commonwealth Scientific and Industrial Research Organization (CSIRO) and Bureau of Meteorology (BOM), Australia—Australian Community Climate and Earth-System Simulator, version 1.3	ACCESS1.3
College of Global Change and Earth System Science, Beijing Normal University—Beijing Normal University Earth System Model	BNU-ESM
Beijing Climate Center, China Meteorological Administration—Beijing Climate Center, Climate System Model, version 1.1	BCC-CSM1.1
Canadian Centre for Climate Modeling and Analysis—Second Generation Canadian Earth System Model	CanESM2
National Center for Atmospheric Research—Community Climate System Model, version 4	CCSM4
Centre National de Recherches Météorologiques (CNRM)/Centre Européen de Recherche et Formation Avancé en Calcul Scientifique—CNRM Coupled Global Climate Model, version 5	CNRM-CM5
Commonwealth Scientific and Industrial Research Organization (CSIRO) in collaboration with Queensland Climate Change Centre of Excellence—CSIRO Mark, version 3.6.0	CSIRO-Mk3.6.0
NOAA Geophysical Fluid Dynamics Laboratory (GFDL)—GFDL Climate Model, version 3	GFDL-CM3
NOAA GFDL—GFDL Earth System Model with Generalized Ocean Layer Dynamics (GOLD) component	GFDL-ESM2G
NOAA GFDL—GFDL Earth System Model with Modular Ocean Model 4 (MOM4) component	GFDL-ESM2M
NASA Goddard Institute for Space Studies (GISS)—GISS Model E, coupled with the Russell ocean model	GISS-E2-R
Met Office Hadley Centre—Hadley Centre Global Environment Model, version 2—Earth System	HadGEM2-ES
Institut Pierre-Simon Laplace (IPSL)—IPSL Coupled Model, version 5, coupled with NEMO, low resolution	IPSL-CM5A-LR
Japan Agency for Marine-Earth Science and Technology (JAMSTEC), Atmosphere and Ocean Research Institute (University of Tokyo), and National Institute for Environmental Studies (NIES)—Model for Interdisciplinary Research on Climate, Earth System Model	MIROC-ESM
Atmosphere and Ocean Research Institute (University of Tokyo), NIES, and JAMSTEC—Model for Interdisciplinary Research on Climate, version 5	MIROC5
Max Planck Institute for Meteorology (MPI)—MPI Earth System Model, low resolution	MPI-ESM-LR
MPI—MPI Earth System Model, medium resolution	MPI-ESM-MR
MPI—MPI Earth System Model, paleo	MPI-ESM-P
Meteorological Research Institute (MRI)—MRI Coupled Atmosphere–Ocean General Circulation Model, version 3	MRI-CGCM3
Norwegian Climate Centre—Norwegian Earth System Model, version 1 (intermediate resolution)	NorESM1-M

tropical albedo changes, on the other hand, span a larger range than observed over the last decade or simulated by the CMIP5 models for preindustrial climate.

The imposed radiative forcing in these experiments is not unlike the annually averaged radiative forcing due to variations in the obliquity of the earth's axis on orbital time scales. For example, high obliquity corresponds to more sunlight in high latitudes and less in low latitudes. However, there are several important differences in the magnitude and the latitudinal structure of the obliquity forcing. The extratropical component of the forcing is farther away from the equator (poleward of 45° latitude), so when averaged over the extratropical Pacific (8°–65°) the range of changes in the TOA net shortwave radiative flux due to obliquity variations is significantly smaller than those in our experiments. As a result, climate model experiments with imposed obliquity variations show very modest SST changes in the tropical band, below 0.5°C (e.g., Lee and Poulsen 2005; Mantsis et al. 2011). A question remains why paleoobservations show much greater SST changes in the tropical band on

orbital time scales, on the order of 2°–3°C (Liu and Herbert 2004). If indeed climate models underestimate cloud albedo feedbacks, then our results may also be relevant to the response of tropical SSTs to orbital forcing.

Throughout this paper we define the mean east–west SST gradient (ΔT) as the averaged SST difference between two big regions in the tropical Pacific—the western tropical Pacific SST (8°S–8°N, 130°E–155°W) and eastern tropical Pacific SST (8°S–8°N, 155°–80°W). We also define ΔT_{uo} as the mean temperature gradient for the upper 50 m of the ocean (averaged over the same spatial regions as ΔT). This definition facilitates the formulation of the idealized energy balance model used to explain our results in section 5. As discussed at the end of section 5 we show that our results also hold if we define the east–west gradient as a contrast between the maximum and minimum temperatures in the west and east along the equator (ΔT_{max}). Table 3 provides a list of the definitions associated with all key variables discussed within this paper.

TABLE 3. Key variables.

Variable	Definition
ΔT	The difference between western tropical Pacific SST (8°S–8°N, 130°E–155°W) and eastern tropical Pacific SST (8°S–8°N, 155°–80°W)
ΔT_{uo}	The difference in mean upper-ocean (depth < 50 m) temperature between the western tropical Pacific (8°S–8°N, 130°E–155°W) and the eastern tropical Pacific (8°S–8°N, 155°W–80°W)
ΔT_e	The difference in local-equilibrium SST between the tropical Pacific (8°S–8°N) and the extratropical Pacific (8°–65°N/S)
$\Delta\alpha$	The difference between extratropical (8°–65°N/S) and tropical (8°S–8°N) albedo within the Pacific basin
ΔT_{max}	The difference between the maximum SST within the western equatorial Pacific (3°S–3°N, 140°–165°E) and the minimum SST within the eastern equatorial Pacific (3°S–3°N, 110°–85°W)

3. The response of the tropics to changes in extratropical cloud albedo

In the first set of experiments we see the east–west SST gradient in the tropical Pacific (ΔT) decrease as extratropical cloud albedo is systematically reduced (Fig. 4, experiments 2–9). We find that the results of these and the subsequent experiments can be best expressed as the dependence of the zonal SST gradient on the meridional albedo contrast (Fig. 4a). Since changes in extratropical albedo affect the total planetary albedo, we also express the results of these experiments as a function of planetary albedo (Fig. 4b); however, our subsequent experiments show that the latter connection is poor across different experimental sets.

The response of the tropical Pacific to decreasing extratropical cloud albedo is consistent with the results of Barreiro and Philander (2008). A lower extratropical cloud albedo increases the amount of shortwave radiation reaching the ocean surface raising the temperature of water subducted in the downwelling regions

of the subtropical cells (Fig. 5c). This extratropical warming translates into the upwelling of warmer subsurface water in the equatorial and coastal upwelling regions, decreasing the zonal SST gradient (Fig. 5d). Consequently, the mean intensity of the atmospheric Walker circulation (Fig. 6a) and the easterly trade winds together with the zonal slope of the equatorial thermocline (Fig. 5d) all decrease in response to a reduction of extratropical cloud albedo. Similarly, the strength of the Hadley circulation decreases together with the meridional SST gradient (Fig. 6b). This reduction in the strength of both Hadley and Walker circulations with ΔT agrees with the results of Brierley et al. (2009) and Brierley and Fedorov (2010) for Pliocene climate.

Figure 7a shows the mean SST field for experiment 9, in which the east–west SST gradient has almost vanished (Fig. 5d). In this extreme case the imposed reduction in extratropical albedo amounts to as much as a 40 W m^{-2} increase in net TOA shortwave radiation over parts of the extratropics (Fig. 3). As a result, SST in the

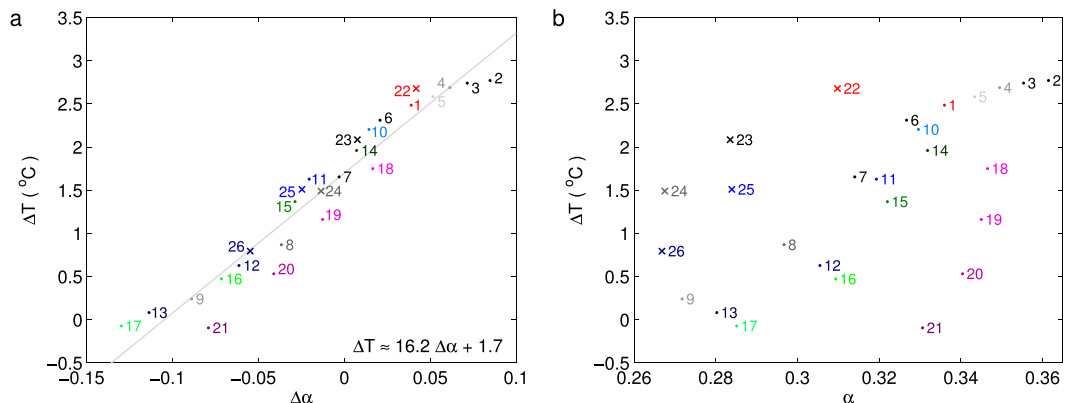


FIG. 4. The east–west SST gradient along the equator in the Pacific Ocean (ΔT) as a function of (a) the Pacific meridional albedo gradient ($\Delta\alpha$) and (b) global albedo (α). The gradient ΔT is defined in Table 3 as indicated by the boxes in Fig. 7. Section 5 provides motivation for considering the zonal SST gradient in terms of such large tropical boxes; a more equatorially confined definition of this gradient is used in Fig. 12. Term $\Delta\alpha$ is defined as in Table 3. Experiments 1 and 22 shown in red are the T31 and 1° controls, respectively.

T31 Pre-industrial Control

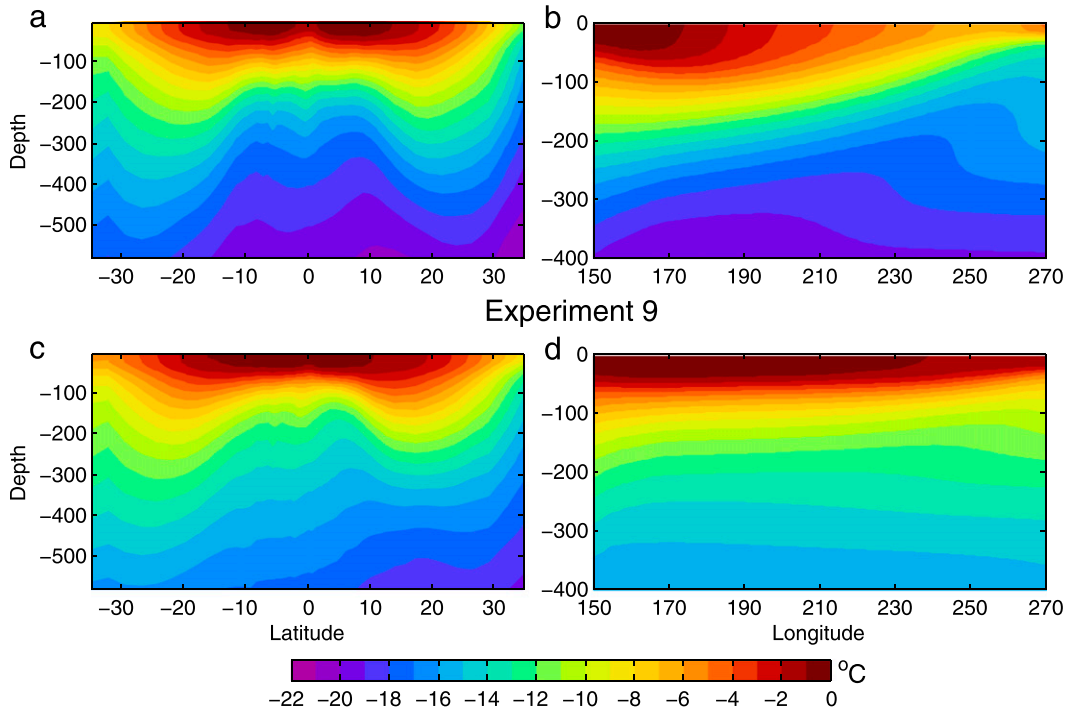


FIG. 5. (left) The zonal mean temperature structure within the Pacific basin and (right) an east–west cross section of upper ocean temperature along 0°N. Temperature is expressed relative to the maximum temperature value within each simulation. (a),(b) The T31 control is contrasted against (c),(d) experiment 9, wherein low extratropical albedo raises the temperature of water subsided in the STCs, decreasing the zonal thermocline slope and SST gradient along the equator.

extratropics and Pacific cold tongue region increases by more than 8°C (Fig. 7b). At the same time, SST in the warm pool increases by only 4°–6°C, resulting in a decrease in ΔT (Figs. 4 and 7b). For the Pacific basin, Fig. 5

compares the zonal mean upper-ocean temperature structure as well as the temperature structure along the equator within experiment 9 against the control. This figure clearly shows warmer waters subsided in the

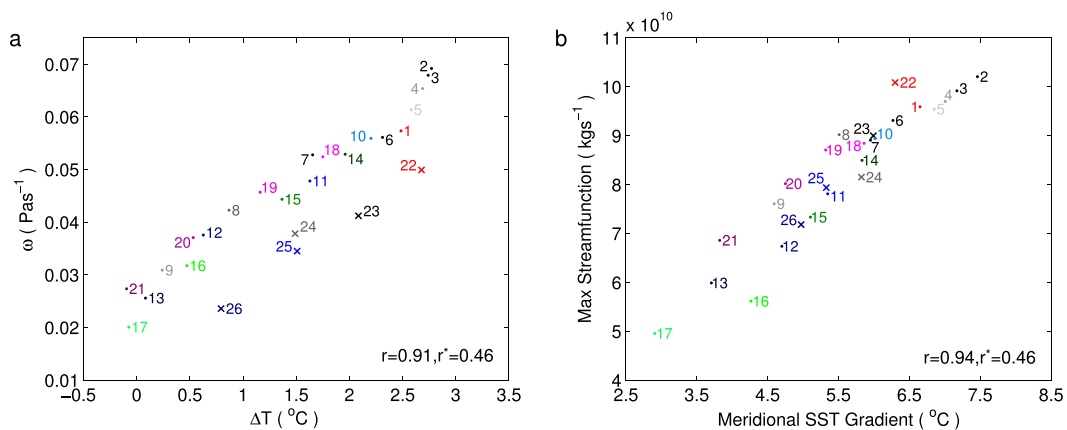


FIG. 6. (a) The Walker circulation strength as a function of the tropical Pacific east–west SST gradient (ΔT). (b) The Hadley circulation strength as a function of the meridional SST gradient. The ΔT is defined as in Table 3. The maximum deviation in ascending pressure velocity (between 130°E and 90°W) from zonal mean values (averaged between 10°S and 10°N) is used as a measure of the Walker cell, and the maximum of the mean atmospheric meridional streamfunction is used as a measure of the Hadley cell. The meridional SST gradient is defined as the difference between tropical (15°S–15°N) and extratropical (40°–20°S, 20°–40°N) ocean temperatures; r indicates the correlation between variables, and r^* the required correlation value for significance at the 95% level taking into account the effective degrees of freedom.

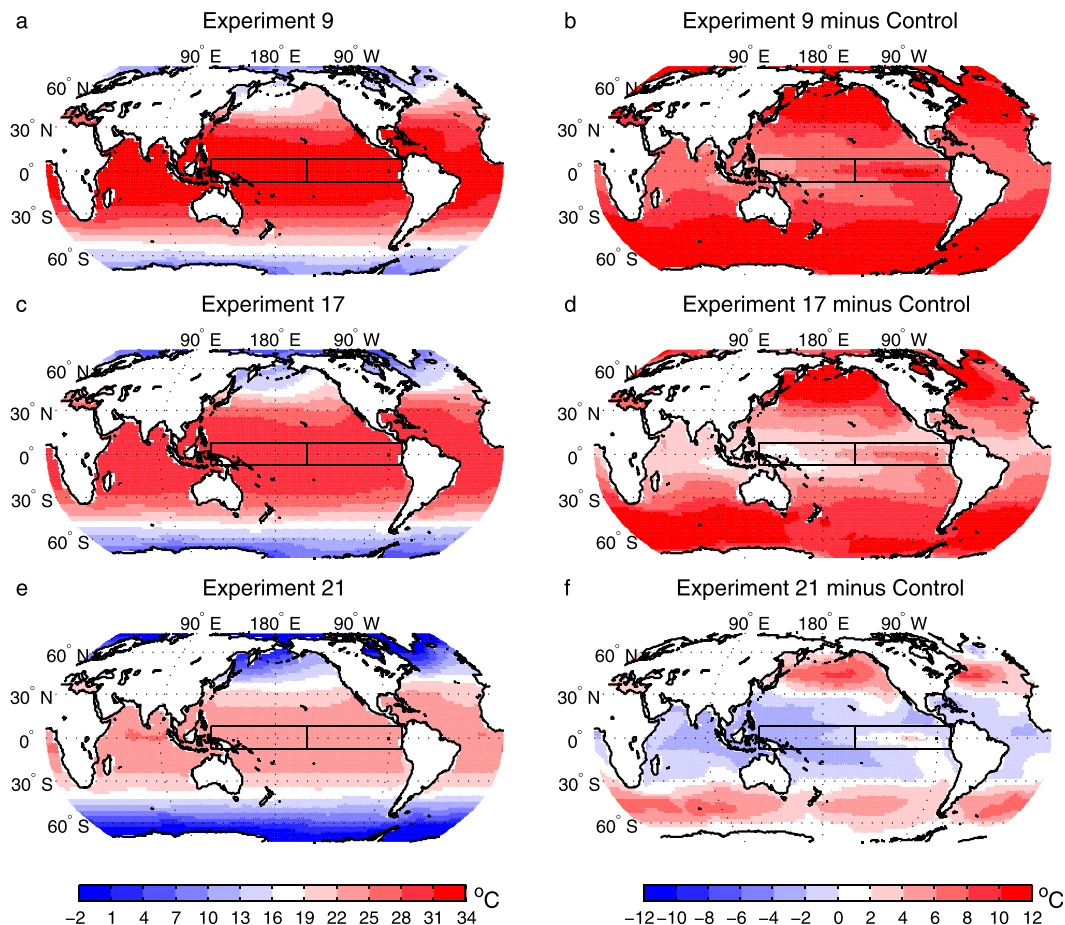


FIG. 7. (left) Mean SST and (right) the SST anomaly with respect to the control in several experiments. (a),(b) Experiment 9: Extratropical cloud albedo has been reduced by 0.072. (c),(d) Experiment 17: Extratropical cloud albedo has been reduced by 0.065 and tropical albedo increased by 0.104. (e),(f) Experiment 21: Extratropical cloud albedo has been reduced by 0.027 and tropical albedo increased by 0.92. For details on the experiments see Table 1. Extratropical albedo is evaluated between 8° and 65° N/S; the tropical albedo between 8° S and 8° N. The numbers quoted are for the Pacific basin.

extratropics and upwelled in the eastern Pacific, resulting in a weaker east–west thermocline tilt.

Further, we find an important albedo compensation that occurs over the tropical Pacific Ocean within this first set of experiments wherein only extratropical albedo is explicitly modified—we observe a change in tropical albedo of the opposite sign to the imposed extratropical albedo change. This unforced tropical compensation occurs in both T31 (set 1 experiments) and 1° (set 4 experiments 23 and 24) configurations; however, its magnitude is weaker for the 1° experiments (see Table 1). In effect, this compensation amounts to a negative feedback for the planetary albedo—the imposed extratropical changes are partially balanced by the climate systems response in the tropical band.

To provide an indication of the spatial structure associated with the resulting unforced tropical albedo changes, Fig. 8 shows simulated albedo anomalies with

respect to the control for T31 experiment 8 (Fig. 8a) as well as for 1° experiment 24 (Fig. 8b). Evident in Fig. 8 is that this unforced tropical compensation is largely due to the eastward expansion of convective cloud across the Pacific. As observed during current-day El Niño events (Ramanathan and Collins 1991; Lloyd et al. 2012), the amount of solar radiation reaching the surface within the tropical Pacific decreases in response to a warming of SST in the eastern Pacific. The magnitude of the compensating tropical albedo change appears to be larger for a given decrease in extratropical albedo than an increase (Fig. 3a and Table 1, experiments 2–5 vs 6–9).

The heat budget perspective provides further clues as to the connection between extratropical albedo and the east–west SST gradient. When extratropical cloud albedo is decreased, the ocean loses less heat in the extratropics and therefore, under the constraint of a balanced heat budget, the ocean must gain less heat within the

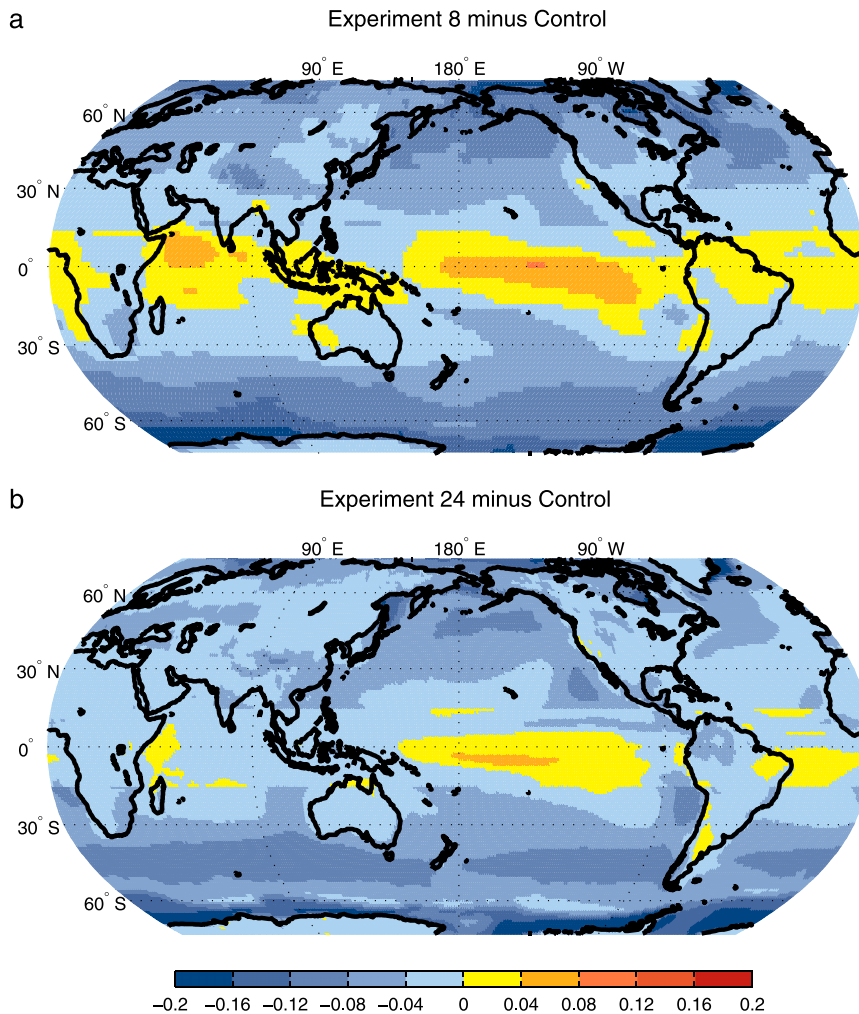


FIG. 8. Anomalies in mean cloud albedo with respect to the control for (a) experiment 8 and (b) experiment 24. These two experiments use the T31 and 1° configurations, respectively. In these perturbation experiments atmospheric water path has been modified but only in the extratropics (poleward of 15°N/S), leading to a reduction in albedo in that region. A compensating (unforced) increase in tropical cloud albedo occurs in response to the imposed extratropical perturbation. A slightly stronger compensation is seen in the coarser model.

tropics. The net surface heat flux into the tropical Pacific Ocean must therefore decrease across experiments 2–9. As shown in Fig. 9a this is indeed the case. This reduction of the net surface heat flux into the tropical Pacific Ocean is achieved across experiments 2–9 as the warm pool and hence the region of convection extends farther eastward when warmer water is upwelled within the eastern Pacific. The zonal asymmetry in cloud forcing (DiNezio et al. 2009) reduces as the east–west SST gradient reduces and conditions in the east become more like the west.

Typically, the surface waters over the warm pool gain less heat because 1) the latent heat flux owing to evaporative cooling is enhanced and 2) the convective clouds

that reside above the warm pool are able to reflect some fraction of incoming solar radiation, reducing its absorption at the ocean surface. In the T31 and 1° control experiments the heat flux into the ocean over the western Pacific warm pool region is $\sim 20 \text{ W m}^{-2}$, whereas in the east, over the cold tongue, it is ~ 80 and $\sim 70 \text{ W m}^{-2}$ for the T31 and 1° control, respectively. As the east becomes more and more like the west in experiments 2 through to 9, and mean tropical Pacific conditions warm, the increased cooling owing to surface evaporative processes is to a large extent balanced by enhanced longwave trapping (note that across experiments 2–9 there is substantial global warming as the global albedo is reduced). Increased tropical cloud

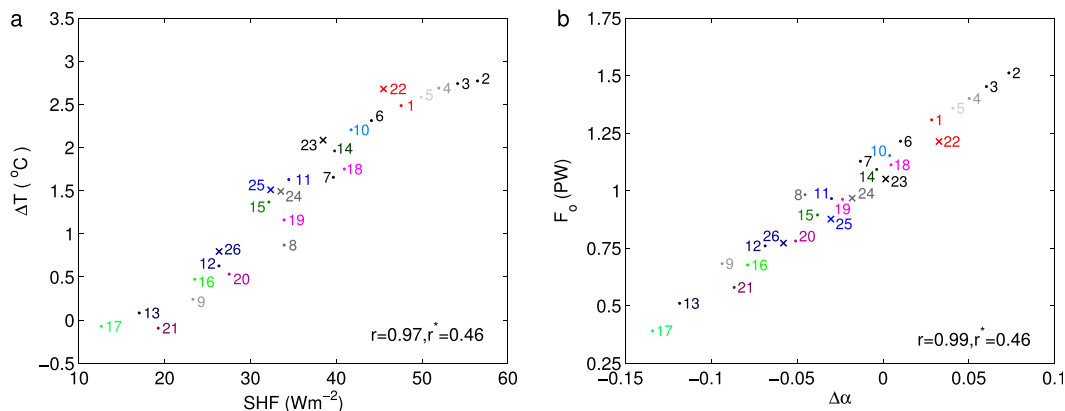


FIG. 9. (a) The east–west SST gradient (ΔT) vs the surface heat flux (SHF) for the tropical Pacific basin. SHF is defined as the mean surface heat flux into the tropical Pacific (8°S – 8°N , 130°E – 80°W). (b) The meridional oceanic heat transport (F_o) out of the tropical Pacific (8°S – 8°N) vs the Pacific meridional albedo gradient ($\Delta\alpha$). Note the nearly perfect linear relationship between $\Delta\alpha$ and the ocean heat transport from the tropical Pacific. The differences ΔT and $\Delta\alpha$ are defined as in Table 3; r indicates the correlation between variables and r^* the required correlation value for significance at the 95% level taking into account the effective degrees of freedom.

albedo therefore plays an important role in the reduction of the net surface heat flux into the tropical Pacific and the associated decrease in the east–west SST gradient.

4. Tropical cloud albedo and the east–west SST gradient

As highlighted in the previous section, ΔT decreases in response to a reduction in extratropical cloud albedo, but the extent of this decrease depends on the magnitude of the albedo response in the tropics to the warming of eastern Pacific SST. To investigate this effect in more detail, in the experiments of sets 2 and 3 we amplify the unforced increase in tropical albedo by imposing an additional increase in cloud albedo within the tropical band (modifying the atmospheric water path).

Let us consider experiments 9, 13, and 17. While the imposed forcing in the extratropics is similar in these experiments, tropical albedo increases from experiment 9 to 13 to 17 (Table 1 and Figs. 3a,b). Increasing tropical albedo acts to reduce the net surface heat flux into the tropical Pacific Ocean (Fig. 9a) and hence the east–west SST gradient (Fig. 4a). Figure 7c shows the mean SST field for experiment 17. The cloud albedo changes imposed in this experiment produce a world that somewhat resembles the early Pliocene in that warm pool temperatures have hardly increased relative to the control (Fig. 7d), yet the meridional and zonal SST gradients have been substantially reduced (Fig. 6).

The enhanced tropical compensation also acts to temper the large decrease in global albedo seen in the set 1 experiments due to the imposed reduction of extratropical

cloud albedo (Fig. 4b). In the set 3 experiments the domain and magnitude of enhanced tropical cloud albedo have been increased relative to the imposed reduction in extratropical albedo—the domain of which now only covers 30° – 60°N/S . This set of experiments was designed to achieve a minimal change in global albedo relative to the T31 control simulation while still reducing the east–west SST gradient (Fig. 4b). Figure 7e shows the mean SST field for experiment 21. The cold tongue together with the east–west SST gradient has vanished. However, owing to the large imposed increase in tropical as well as subtropical (30°S – 30°N) cloud albedo within this experiment (Fig. 3c), warm pool temperatures have decreased relative to the control (Fig. 7f). Tropical cloud albedo acts to regulate tropical Pacific heat gain and therefore the east–west SST gradient and the temperature of the warm pool.

One thing all of these experiments have in common is that decreasing extratropical albedo and increasing tropical albedo reduces the east–west SST gradient. A corollary of these results implies that a strong relationship exists between the meridional gradient in cloud albedo ($\Delta\alpha$) and the strength of the zonal SST gradient (ΔT); see Fig. 4a. This strong relationship stands in a stark contrast to the very weak dependence between the east–west SST gradient along the equator and planetary albedo (Fig. 4b).

The correspondence between $\Delta\alpha$ and ΔT can be viewed from two perspectives. From the first perspective, the temperature of water upwelled within the eastern Pacific, the SST in the cold tongue, and therefore the extent of tropical Pacific convective clouds, are largely controlled by extratropical albedo. Then, depending on the magnitude of the tropical albedo response to the warming

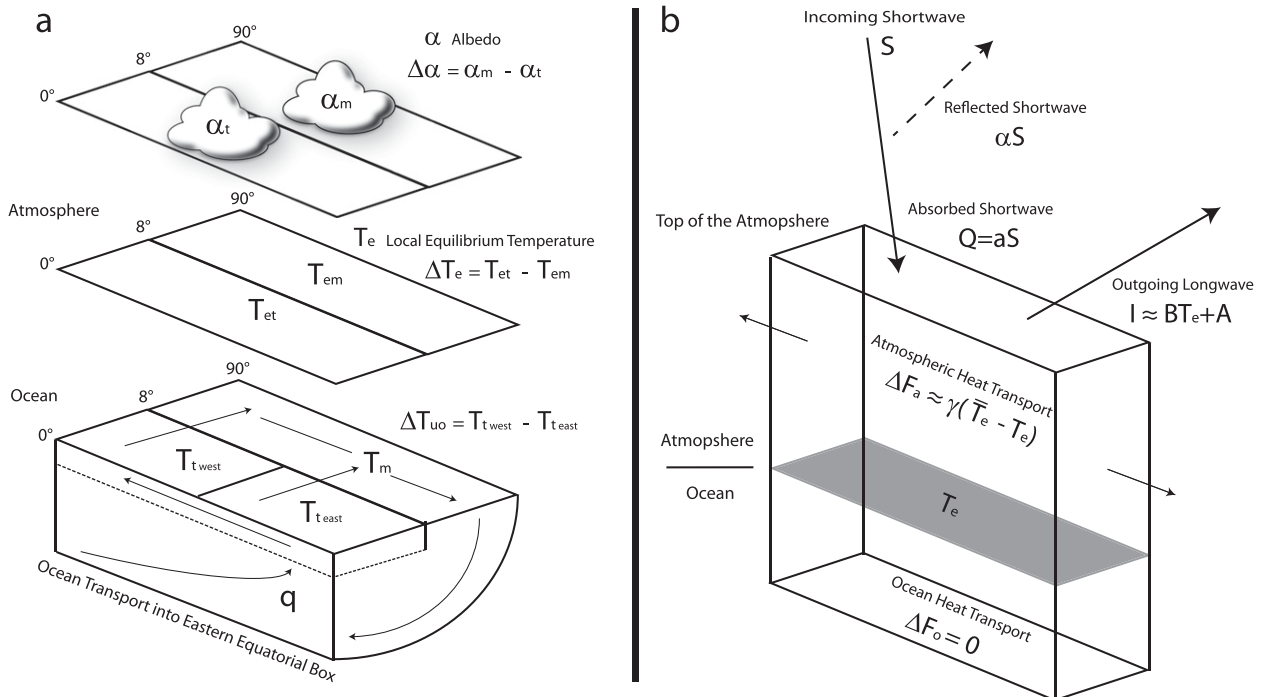


FIG. 10. (a) A schematic of the idealized analytical model for the warm pool, cold tongue, and Walker circulation complex (WCWC) adapted from Fig. 1 in Liu and Huang (1997). All temperatures and albedo values are given as averages over the specified regions. Indices m and t stand for the midlatitudes (extratropics) and tropics, respectively; q indicates the ocean heat transport into the eastern equatorial box. (b) The simple energy balance model, akin to that of Budyko (1969), employed to estimate local-equilibrium SSTs, T_{em} and T_{et} , defined here as temperatures that the ocean would have in the absence of oceanic heat transport. Outgoing longwave radiation is represented as a linear function of the local-equilibrium temperature. Atmospheric heat transport is parameterized as a linear function of the difference between global mean and local surface temperatures.

of the cold tongue, the surface heat flux into the tropical Pacific, and as a result ΔT , decreases (Fig. 9a). From a more global perspective, a reduction in the albedo contrast between the extratropics and the tropics implies that the former now receive more shortwave radiation while the latter less radiation relative to the present-day climate. Consequently, the required equator-to-pole heat transport of the fully coupled ocean–atmosphere system is reduced. Consistent with the theoretical arguments of Held (2001), the partitioning of the zonally averaged poleward heat transport between the atmosphere and the Pacific Ocean remains roughly the same across the experiments conducted (not shown), so it follows that the required net ocean heat transport from the tropical Pacific is reduced as well. This is accomplished by a weakening of the cold tongue and, hence, a reduction in tropical Pacific Ocean heat uptake for smaller values of $\Delta\alpha$ (Fig. 9b). These two views are united by the constraint of a balanced heat budget—in the steady state the net surface heat flux into the tropical Pacific Ocean is balanced by the net ocean heat transport out of the tropical Pacific.

5. The meridional albedo gradient sets the zonal SST gradient: A simple model

The main result emerging from these simulations is that, rather than purely the magnitude of extratropical cloud albedo (Barreiro and Philander 2008), it is the meridional gradient in albedo ($\Delta\alpha$) that sets the strength of the zonal SST gradient (ΔT) within the tropical Pacific (Fig. 4a). Next, we will account for the scaling of ΔT with $\Delta\alpha$ by considering an analytical model for the warm pool, cold tongue, and Walker circulation complex (WCWC), similar to that of Liu and Huang (1997) (Fig. 10a), combined with an energy balance model for local-equilibrium temperature (Budyko 1969) (Fig. 10b).

Liu and Huang (1997) find that, because of saturation, in a steady state the east–west upper-ocean temperature gradient in the tropical band cannot exceed an upper bound set by surface equilibrium temperatures and regulated by ocean currents. This upper bound is equal approximately to a quarter of the difference between local-equilibrium SSTs in the tropics and the extratropics:

$$\Delta T_{\text{uo}} \leq 0.25 \Delta T_e. \quad (1)$$

Here ΔT_{uo} is defined as the difference in mean upper-ocean (depth < 50 m) temperature between the western (130°E–155°W) and eastern (155°–85°W) tropical Pacific. Also, $\Delta T_e = T_{\text{et}} - T_{\text{em}}$, where T_{et} is the local-equilibrium SST for the tropical Pacific and T_{em} is the local-equilibrium SST for the extratropical Pacific. These local-equilibrium temperatures are defined here as the SST that would be realized in the absence of oceanic circulation (and hence with zero heat transport by the ocean). The boundaries between the tropics and the extratropics are chosen as 8°N and 8°S. In the box model of Liu and Huang (1997) ΔT_e represents the meridional gradient in the temperature toward which the ocean is being restored by surface heat fluxes. Unlike conventional radiative–convective equilibrium temperature above the ocean surface, T_{et} and T_{em} depend on the efficiency of atmospheric heat transport as well as the TOA heat flux and optical thickness of the atmosphere. The gradient of ΔT_e is established by the response of the coupled ocean–atmosphere system—within our experiments it is determined by the response of the coupled system to a change in the optical properties of clouds.

Within the realistic range of parameters this saturation west–east temperature difference actually lies between $0.2 \Delta T_e$ and $0.3 \Delta T_e$ and is achieved at a modest coupling strength between equatorial SSTs, trade winds, and ocean transport, with the coefficient 0.25 giving the best estimate (Liu and Huang 1997). The saturation ΔT_{uo} is reached when the ocean surface currents generated by dynamic ocean–atmosphere coupling (via the Walker and Hadley circulations) are strong enough such that the advection time scale becomes comparable to the local thermodynamic relaxation time scale. At this point advection due to ocean currents acts to reduce rather than increase the east–west SST gradient and the maximum ΔT_{uo} is reached. Liu and Huang suggest that the Pacific today has reached this saturation state and that the mean east–west temperature gradient in the upper ocean is primarily determined by the meridional gradient in the temperature toward which the ocean is being restored in their model (ΔT_e).

To estimate ΔT_e we employ a simple energy balance model akin to that of Budyko (1969) (see also Held and Suarez 1974). In the steady state, and assuming no horizontal heat transport by the ocean, the vertically integrated energy balance at any given point on the earth's surface is defined as

$$Q - I + \Delta F_a = 0, \quad (2)$$

where $Q = aS$ is the absorbed solar radiation, S being the TOA incoming solar radiation and a the coalbedo ($a = 1 - \alpha$); I represents the outgoing longwave radiation at the TOA and ΔF_a the energy gain due to the convergence of horizontal atmospheric heat transport (Budyko 1969; Held and Suarez 1974; Hartmann 1994).

In (2), I is parameterized as a linear function of surface temperature (T):

$$I = BT + A, \quad (3)$$

where $B = 1.7 \text{ W m}^{-2} \text{ } ^\circ\text{C}^{-1}$, as estimated by Rose and Marshall (2009) using a linear regression between long-term mean outgoing longwave radiation and 1000-hPa temperature in the National Centers for Environmental Prediction (NCEP) reanalysis product. This value for B is close to that obtained from the best linear fit between mean values of I and T for every model grid point within all of the T31 and 1° simulations performed in the present study (Fig. 11a): B is determined primarily by the Stefan–Boltzmann and water vapor feedbacks (Hartmann 1994; Held and Shell 2012).

In (3), A is set such that for the global average

$$\bar{a}\bar{S} = B\bar{T} + A \quad (4)$$

with \bar{S} , \bar{a} , and \bar{T} representing global mean values.

In (2), ΔF_a is parameterized as a linear function of the difference between global mean and local surface temperature:

$$\Delta F_a = \gamma(\bar{T} - T), \quad (5)$$

where γ represents the efficiency of the atmosphere in transporting energy poleward. To obtain a value for this parameter we consider the best linear fit between mean values of ΔF_a and $\bar{T} - T$ for every model grid point equatorward of 65°N/S within all of the simulations performed (Fig. 11b). Based on this fit γ is estimated here as $\gamma = 3.3 \text{ W m}^{-2} \text{ } ^\circ\text{C}^{-1}$.

Equation (2) becomes

$$aS - BT - A + \gamma(\bar{T} - T) = 0. \quad (6)$$

Assuming $\bar{a}\bar{S} \approx \bar{a}\bar{S}$ when averaging over the tropical and extratropical Pacific, T_{et} and T_{em} can be estimated using Eq. (6) such that

$$T_{\text{et}} = \frac{a_t S_t}{B + \gamma} + \frac{\gamma \bar{T}}{B + \gamma} - \frac{A}{B + \gamma} \quad (7)$$

and

$$T_{\text{em}} = \frac{a_m S_m}{B + \gamma} + \frac{\gamma \bar{T}}{B + \gamma} - \frac{A}{B + \gamma} \quad (8)$$

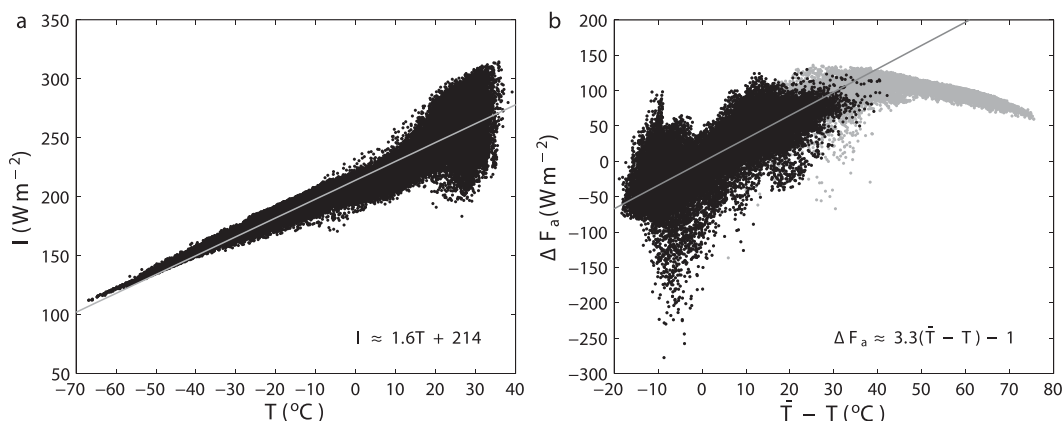


FIG. 11. Estimations of parameters B and γ for the energy balance model using the best linear fit between mean values for every model grid point within all of the simulations performed (both the T31 and 1° configurations). (a) The mean TOA outgoing longwave radiation I vs surface temperature T . (b) The mean energy gain due to horizontal atmospheric heat transport (ΔF_a) vs local surface temperature deviation from the global mean value ($\bar{T} - T$). In (b) the best linear fit is based on every model grid point equatorward of 65°N/S (black shading) while the grid points poleward of 65°N/S have been excluded (gray shading).

in which S_t and S_m are the TOA incoming solar radiation averaged over the tropical (8°S – 8°N) and extratropical (8° – 65°N/S) Pacific, respectively, and a_t and a_m are the coalbedo.

We can now consider changes in the meridional gradient in local-equilibrium SST ($\Delta T'_e$) in terms of albedo changes:

$$\begin{aligned} \Delta T'_e &= T'_{\text{et}} - T'_{\text{em}} \\ &= \frac{1}{B + \gamma} a'_t S_t - \frac{1}{B + \gamma} a'_m S_m. \end{aligned} \quad (9)$$

The tropical and extratropical Pacific TOA incoming solar radiation can be decomposed into $S_t = \bar{S}_{\text{pac}} + \tilde{S}_t$ and $S_m = \bar{S}_{\text{pac}} + \tilde{S}_m$, where \bar{S}_{pac} represents the mean TOA incoming solar radiation over the entire Pacific basin. Substituting these decompositions into Eq. (9) yields

$$\begin{aligned} \Delta T'_e &= \frac{1}{B + \gamma} a'_t (\bar{S}_{\text{pac}} + \tilde{S}_t) - \frac{1}{B + \gamma} a'_m (\bar{S}_{\text{pac}} + \tilde{S}_m) \\ &= \frac{1}{B + \gamma} \bar{S}_{\text{pac}} \Delta a' + \frac{1}{B + \gamma} a'_t \tilde{S}_t - \frac{1}{B + \gamma} a'_m \tilde{S}_m \\ &\approx \frac{\bar{S}_{\text{pac}}}{B + \gamma} \Delta a' \\ &\approx 76 \Delta a', \end{aligned} \quad (10)$$

where $\bar{S}_{\text{pac}} = 382 \text{ W m}^{-2}$. The terms $(B + \gamma)^{-1} a'_t \tilde{S}_t$ and $(B + \gamma)^{-1} a'_m \tilde{S}_m$ are small in comparison to $(B + \gamma)^{-1} \bar{S}_{\text{pac}} \Delta a'$ (on the order of $\sim 4\%$ of the total). The meridional gradient in equilibrium temperature is therefore tightly related to the meridional gradient in Pacific

albedo as confirmed by Fig. 12a. The slope of the best linear fit, 77°C , falls close to our estimate of $\Delta T'_e \approx 76 \Delta a'$ (since $\Delta a' = a_t - a_m = -\alpha_t + \alpha_m = \Delta \alpha'$).

Matching the theoretical predictions, our experimental results confirm that, indeed, ΔT_{uo} approaches saturation values within all of the experiments conducted. The slope of the best linear fit agrees well with $\Delta T'_{\text{uo}} \approx 0.25 \Delta T'_e$ (Fig. 12b). Although the strength of the Hadley and Walker cells (Fig. 6), the strength of surface easterly winds, and the volume transport by the STCs all decrease as the meridional gradient in local-equilibrium SST (ΔT_e) is decreased, the experiments all stay within the saturation regime for two reasons. First, the surface heat flux restoring time scale generally increases together with the advection time scale as the meridional gradient in local-equilibrium SST (ΔT_e) is decreased. Second, a background meridional temperature gradient persists within our realistic fully coupled simulations even once $\Delta T_e \approx 0$. Even the experiments wherein the meridional gradient in local-equilibrium SST (ΔT_e) as well as the zonal temperature gradient (ΔT_{uo}) are approximately zero (i.e., experiments 13 and 17) do not equate to a collapsed ocean circulation and local thermal equilibrium because, unlike the simple box model, a background meridional temperature gradient persists within our realistic fully coupled simulations. The Hadley circulation, although significantly weaker than in the control (Fig. 6b), still supports wind-driven meridional oceanic circulation within the subtropical cells, allowing for nonzero heat uptake by the ocean in the equatorial band and ocean heat transport out of the tropical Pacific (Fig. 9).

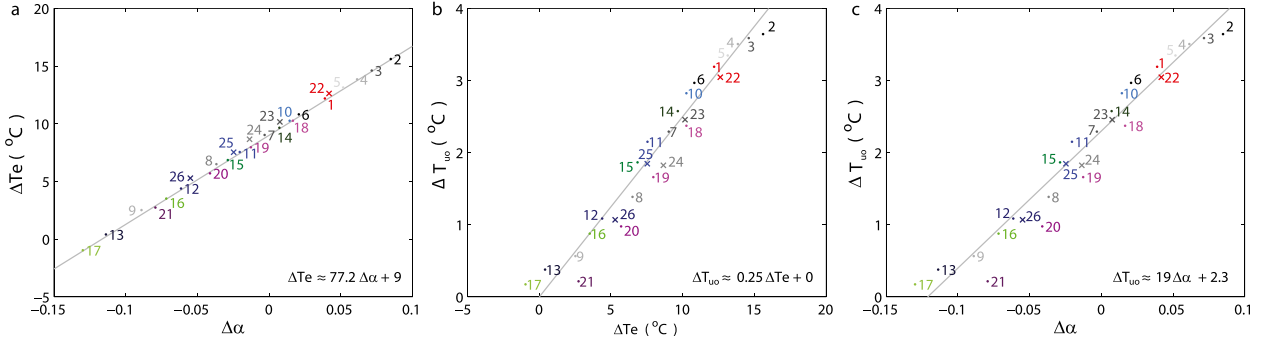


FIG. 12. Linking the zonal upper-ocean temperature gradient to the meridional albedo gradient. (a) The meridional gradient in local-equilibrium SST (ΔT_e) vs the Pacific meridional albedo gradient ($\Delta\alpha$). (b) The tropical Pacific east–west upper-ocean temperature gradient (ΔT_{uo}) vs the meridional gradient in local-equilibrium SST (ΔT_e). (c) The east–west upper-ocean temperature gradient (ΔT_{uo}) vs the Pacific meridional albedo gradient ($\Delta\alpha$). Terms $\Delta\alpha$, ΔT_e , and ΔT_{uo} are defined as in Table 3. The linear relationship between ΔT_{uo} and $\Delta\alpha$ in the right panel is a consequence of the tight linear relationships between relevant variables in the first two panels.

Finally we arrive at an expression for the zonal upper-ocean temperature gradient in terms of the meridional albedo gradient:

$$\Delta T'_{uo} \approx 0.25 \Delta T'_e \approx 0.25 \frac{\bar{S}_{pac}}{B + \gamma} \Delta\alpha' \approx 19 \Delta\alpha'. \quad (11)$$

Hence, this expression explains the linear relationship between the zonal upper-ocean temperature gradient and the meridional albedo gradient within the Pacific (Fig. 12c). As shown in Fig. 12c the slope of the best linear fit falls close to this estimate. Given that ΔT_{uo} is near its saturation value, Eq. (11) indicates that the scaling of ΔT_{uo} with $\Delta\alpha$ depends on 1) the mean TOA incoming solar radiation over the Pacific basin (\bar{S}_{pac}) and 2) how efficiently this energy is either transported away by the atmosphere (γ) or radiated back to space (B). This scaling also suggests that, if two GCMs (forced with the same TOA solar forcing) maintain the same Pacific meridional albedo gradient, then their zonal Pacific SST gradients can differ only to the extent that the efficiency of their atmospheric components differ in radiating and transporting heat.

The slope of the best linear fit between ΔT_{uo} and $\Delta\alpha$ ($\Delta T'_{uo} \approx 19 \Delta\alpha'$, Fig. 12c) is greater than between ΔT and $\Delta\alpha$ ($\Delta T' \approx 16 \Delta\alpha'$, Fig. 4a). We ascribe this to the stronger effect of homogenizing atmospheric damping relative to ocean dynamics at the surface.

In Fig. 13a the observed relationship between $\Delta\alpha$ and ΔT_{uo} , as well as the relationship within 20 CMIP5 simulations of preindustrial climate, has been added to the results of our modified water path experiments. We find that the strong linear relationship between $\Delta\alpha$ and ΔT_{uo} still holds for this broad selection of models. The best linear fit between $\Delta\alpha$ and ΔT_{uo} once the CMIP5 simulations and observations have been added is

$\Delta T'_{uo} \approx 19.6 \Delta\alpha'$, falling close to the scaling estimate provided by Eq. (11). If we only consider the CMIP5 models, $\Delta T'_{uo} \approx 7.9 - 19.3 \Delta\alpha'$ within the 95% confidence bounds. We expect this scaling to be somewhat model dependent, differing among the CMIP5 models to the extent that the efficiency of their atmospheric components differ in radiating and transporting heat.

Throughout this paper we have defined the east–west SST gradient (ΔT) as the difference between western (8°S–8°N, 130°E–155°W) and eastern (8°S–8°N, 155°–80°W) tropical Pacific SST as indicated by the boxes in Figs. 7 and 13b and Table 3. We have used this definition because, as the surface expression of ΔT_{uo} (Table 3), it is the most consistent with the idealized WCWC box model. However, this relationship between the meridional albedo gradient and the zonal SST gradient still holds even if we focus solely on the equatorial region. Figure 14a shows the relationship between $\Delta\alpha$ and ΔT_{max} where the latter is defined as the maximum SST contrast along the equator (Table 3; Fig. 14b). The strong linear relationship between $\Delta\alpha$ and the zonal SST gradient remains. The slope between $\Delta\alpha$ and the east–west SST gradient is now, however, much steeper than in Fig. 4a as we have moved away from the box averages.

6. Conclusions

In this study we have demonstrated how the gradient in cloud albedo between the tropics and midlatitudes ($\Delta\alpha$) can set the mean east–west sea surface temperature gradient in the tropical Pacific (ΔT). Within a suite of numerical experiments conducted with a comprehensive GCM we have observed a tight linear relationship between the two variables. Control simulations of CMIP5 appear to follow the same dependence (Figs. 13 and 14).

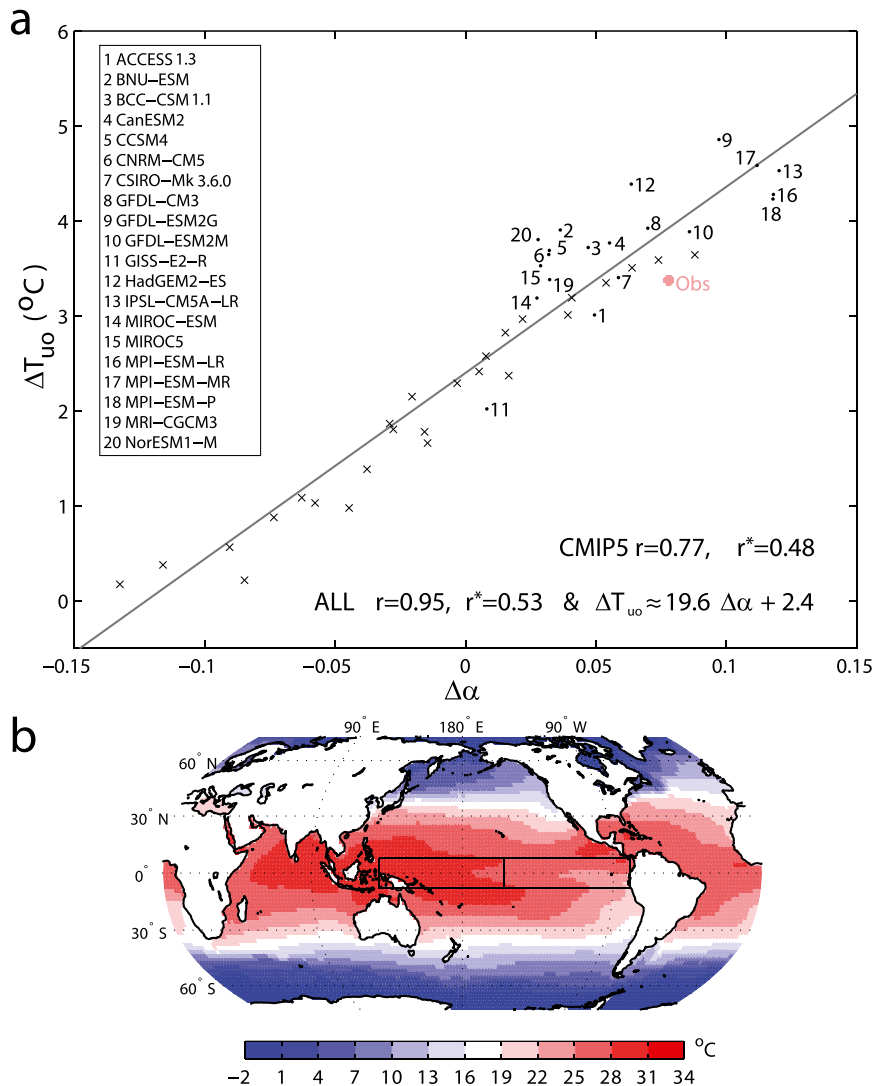


FIG. 13. (a) The east-west upper-ocean temperature gradient (ΔT_{uo}) as a function of the Pacific meridional albedo gradient ($\Delta\alpha$). This plot combines results from the preindustrial CMIP5 runs (black dots), our CESM experiments (gray crosses), and observations (red dot); ΔT_{uo} and $\Delta\alpha$ are defined as in Table 3. (b) The regions used to evaluate ΔT_{uo} are shown as boxes superimposed on the present-day observed SST field. The observed values of $\Delta\alpha$ and ΔT_{uo} are based on the CERES-EBAF and WOA2009 datasets, respectively. Coefficient r indicates the correlation between variables and r^* the required correlation value for significance at the 95% level taking into account the effective degrees of freedom.

To account for the scaling of ΔT with $\Delta\alpha$ we have invoked the results of an analytical model of the warm pool, cold tongue, and Walker circulation complex together with a simple energy balance model to estimate the difference in local-equilibrium SST between the tropics and the extratropics. This scaling hinges on three arguments: 1) that the Pacific remains near its saturation state under a wide range of climates, such that the mean east-west SST gradient is primarily determined by the meridional gradient in the local-equilibrium SST; 2) that the relationship between

surface temperature and outgoing longwave radiation at the TOA, and 3) the efficiency of the atmosphere in transporting energy poleward remain approximately constant across a range of climates. As long as these conditions are satisfied (which is true for our experiments), this simple model is able to reproduce the linear relationship between ΔT with $\Delta\alpha$. According to this model, the coefficient connecting the former to the latter is inversely proportional to the efficiency of the atmosphere in transporting heat or radiating it back to space.

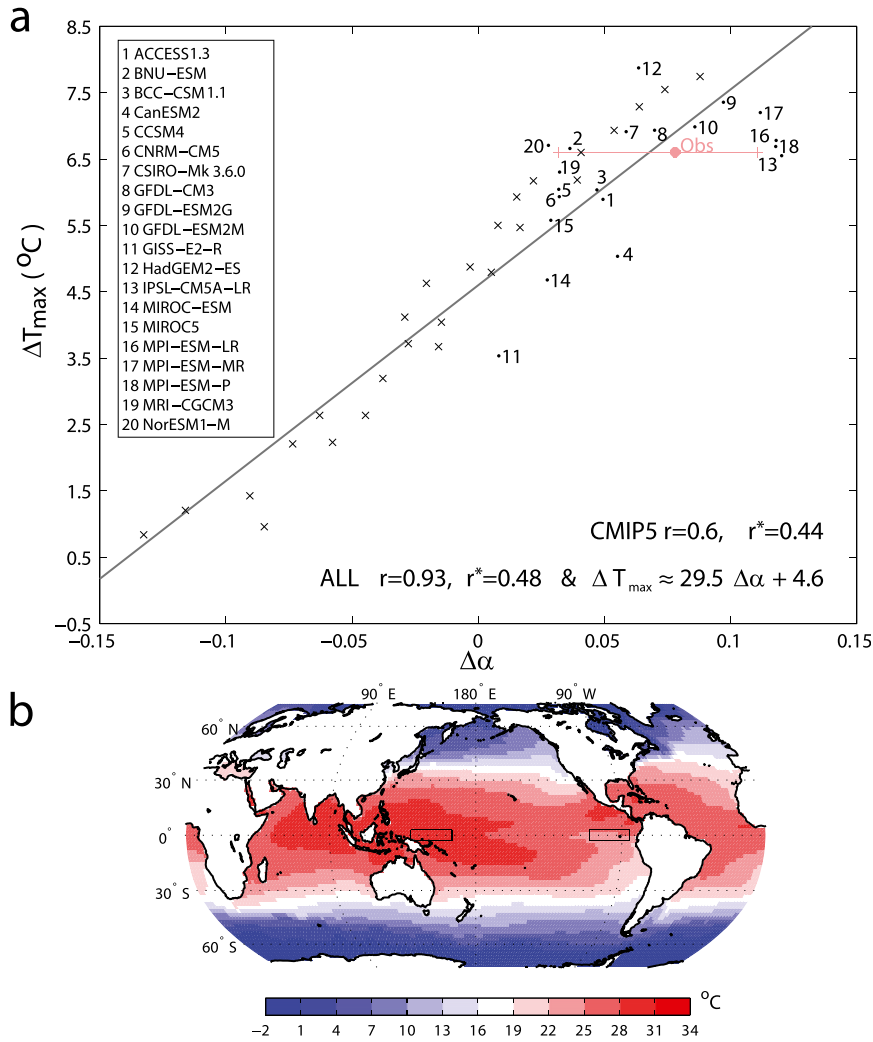


FIG. 14. (a) The east–west SST gradient along the equator (ΔT_{max}) as a function of the Pacific meridional albedo gradient ($\Delta\alpha$). This plot combines results from the preindustrial CMIP5 runs (black dots), our CESM experiments (gray crosses), and observations (red dot with the interannual range for $\Delta\alpha$). The ΔT_{max} and $\Delta\alpha$ are defined as in Table 3; ΔT_{max} is a more equatorial confined zonal SST gradient representing the difference between the maximum SST within the center of the present-day western Pacific warm pool and the minimum SST within the center of the present-day eastern Pacific cold tongue. (b) These regions are shown as boxes superimposed on the present-day observed SST field. The observed values of $\Delta\alpha$ and ΔT_{max} are based on the CERES-EBAF and OISST datasets, respectively. The spread between CMIP5 models is slightly larger here than in Fig. 11 because of differences in the spatial structure of the cold tongue and warm pool between the models. Coefficient r indicates the correlation between variables and r^* the required correlation value for significance at the 95% level taking into account the effective degrees of freedom.

Studies (e.g., Sun and Zhang 2006; Liang et al. 2012) suggest that changes in the properties of ENSO, via the rectification effect of ENSO events into the mean, play a role in controlling the mean state of the tropical Pacific. An investigation into whether changes in ENSO properties are associated with the mean state changes across our simulations is, however, beyond the scope of this current study.

Changes in the gradient in cloud albedo between the tropics and midlatitudes present a mechanism for long-term changes in the east–west tropical Pacific SST gradient and associated Walker circulation that is directly relevant to studies of both future and past climates. Our experiments suggest that the Walker circulation will decrease in response to a reduction in extratropical

albedo, as warmer water is upwelled in the east and convection shifts eastward, occurring more uniformly across the tropical Pacific basin. At the same time the strength of Hadley circulation is also reduced in response to the associated weakening of the meridional SST gradient.

Using an idealized atmospheric GCM, Merlis and Schneider (2011) have demonstrated how, under the assumptions of constant Q flux (representing constant ocean heat transport) and no clouds, the east–west SST gradient should decrease as climate warms owing to “evaporative damping” (Knutson and Manabe 1995). However, for such a mechanism to have substantial impact the climate has to change significantly—a 30% reduction in ΔT would require global mean temperature to increase by some 10°C (Fig. 2 of Merlis and Schneider 2011). In the present study we show that in the fully coupled system changes of the east–west SST gradient are inherently linked to changes in ocean heat transport and cloud cover, which allows for a reduction of ΔT without large changes in global mean temperatures.

The results obtained in this study agree well with the theory of Boccaletti et al. (2004) and Fedorov et al. (2004), based on a balanced heat budget argument. The gradient ΔT is seen to be strongly linked to the intensity of the surface heat flux into the tropical Pacific, which in the steady state amounts to the transport of heat out of the tropics by the Pacific Ocean. As ΔT decreases, the tropical Pacific heat budget is more locally balanced. However, within our realistic fully coupled simulations, when the meridional gradient in local-equilibrium SST, and hence the zonal gradient in upper ocean temperature, approaches zero, oceanic circulation does not fully collapse, and the system does not reach local thermal equilibrium. A nonzero meridional temperature gradient still exists within these simulations, supporting the Hadley circulation, nonzero wind stress forcing, circulation within the subtropical cells (STCs), and weak meridional ocean heat transport. The present study shows that the gradient in cloud albedo between the tropical and extratropical Pacific is a key parameter controlling the ocean heat transport out of the Pacific and hence the mean east–west SST gradient. An inference is that differences in the mean east–west SST gradient within different preindustrial GCM simulations are associated primarily with differences in their oceanic meridional heat transport from the tropics.

We emphasize that this study focuses on oceanic thermal gradients, relating them to the meridional gradient in absorbed solar radiation. Wind-driven poleward ocean heat transport is, however, also influenced by the meridional density gradient, and hence salinity changes can play an important role. For example, a substantial

reduction in the meridional density gradient in the Pacific caused by a strong freshening of surface waters in the extratropics could lead to the collapse of the equatorial thermocline, wiping out the zonal SST gradient completely (Fedorov et al. 2004; Fedorov 2007).

Our results suggest that correctly capturing the cloud albedo response to anthropogenic forcing may be an important factor in determining the response of the mean east–west gradient (to be reported elsewhere). Large differences are seen, however, in the effects of clouds on shortwave radiation in the response of GCMs to anthropogenic forcing (Bony et al. 2006; Bender 2011). With respect to past climates, the results shown within this paper provide an indication of the spatial extent and magnitude of the cloud albedo changes and radiative fluxes required to shift between today and warm worlds such as the early Pliocene. The experiments performed in this study suggest that to reduce the east–west equatorial SST gradient down to the small values typical of the Pliocene epoch, a reversal of the meridional albedo gradient over the Pacific Ocean may be required. That is, clouds in the extratropics should become on average less reflective than those in the equatorial band. Whether this scenario is realistic remains to be seen—in the present-day climate, interannual albedo variations between March 2000 and June 2012 do reduce this gradient to near zero at times, but do not reverse its sign (Fig. 14). Subsequent questions lie in exploring the feasibility and possible cause of the required albedo change, such as changes in atmospheric aerosols.

Acknowledgments. This research is supported by grants from the Department of Energy Office of Science (DE-SC0007037) and the David and Lucile Packard Foundation. The CESM project is supported by the National Science Foundation and the Department of Energy Office of Science. Computations were performed at the Yale University. Faculty of Arts and Sciences High Performance Computing Center. We acknowledge the World Climate Research Programme’s Working Group on Coupled Modelling, which is responsible for CMIP, and we thank the modeling groups (listed in Table 2 of this paper) for making available their model output. For CMIP the Department of Energy’s Program for Climate Model Diagnosis and Intercomparison provides coordinating support and led development of software infrastructure in partnership with the Global Organization for Earth System Science Portals. Les Muir is gratefully acknowledged for his assistance in obtaining the CMIP data used in this study. We thank Chris Briery and Brian Dobbins for their advice in setting up the CESM simulations, and George Philander, Georgy Manucharyan, and Jeff Carpenter for insightful discussions on

this work. Finally, we thank the reviewers of this paper for their very constructive feedback.

REFERENCES

- Allan, R., A. Slingo, and M. Ringer, 2002: Influence of dynamics on the changes in tropical cloud radiative forcing during the 1998 El Niño. *J. Climate*, **15**, 1979–1986, doi:10.1175/1520-0442(2002)015<1979:IODOTC>2.0.CO;2.
- Barreiro, M., and S. G. Philander, 2008: Response of the tropical Pacific to changes in extratropical clouds. *Climate Dyn.*, **31**, 713–729, doi:10.1007/s00382-007-0363-5.
- , —, R. Pacanowski, and A. Fedorov, 2006: Simulations of warm tropical conditions with application to middle Pliocene atmospheres. *Climate Dyn.*, **26**, 349–365, doi:10.1007/s00382-005-0086-4.
- Bender, F., 2011: Planetary albedo in strongly forced climate, as simulated by the CMIP3 models. *Theor. Appl. Climatol.*, **105**, 529–535, doi:10.1007/s00704-011-0411-2.
- Bjerknes, J., 1969: Atmospheric teleconnections from the equatorial Pacific. *Mon. Wea. Rev.*, **97**, 163–172, doi:10.1175/1520-0493(1969)097<0163:ATFTEP>2.3.CO;2.
- Boccaletti, G., R. C. Pacanowski, S. G. H. Philander, and A. V. Fedorov, 2004: The thermal structure of the upper ocean. *J. Phys. Oceanogr.*, **34**, 888–902, doi:10.1175/1520-0485(2004)034<0888:TTSOTU>2.0.CO;2.
- Bony, S., and Coauthors, 2006: How well do we understand and evaluate climate change feedback processes? *J. Climate*, **19**, 3445–3482, doi:10.1175/JCLI3819.1.
- Brierley, C. M., and A. V. Fedorov, 2010: Relative importance of meridional and zonal sea surface temperature gradients for the onset of the ice ages and Pliocene–Pleistocene climate evolution. *Paleoceanography*, **25**, PA2214, doi:10.1029/2009PA001809.
- , —, Z. Liu, T. D. Herbert, K. T. Lawrence, and J. P. LaRiviere, 2009: Greatly expanded tropical warm pool and weakened Hadley circulation in the early Pliocene. *Science*, **323**, 1714–1718, doi:10.1126/science.1167625.
- Budyko, M. I., 1969: The effect of solar radiation variations on the climate of the earth. *Tellus*, **21**, 611–619, doi:10.1111/j.2153-3490.1969.tb00466.x.
- Cess, R., M. Zhang, B. Wielicki, D. Young, X.-L. Zhou, and Y. Nikitenko, 2001: The influence of the 1998 El Niño upon cloud-radiative forcing over the Pacific warm pool. *J. Climate*, **14**, 2129–2137, doi:10.1175/1520-0442(2001)014<2129:TIOTEN>2.0.CO;2.
- Chen, J., B. Carlson, and A. D. Del Genio, 2002: Evidence for strengthening of the tropical general circulation in the 1990s. *Science*, **295**, 838–841, doi:10.1126/science.1065835.
- Clement, A., R. Seager, and R. Murtugudde, 2005: Why are there tropical warm pools? *J. Climate*, **18**, 5294–5311, doi:10.1175/JCLI3582.1.
- Collins, M., 2005: El Niño- or La Niña-like climate change? *Climate Dyn.*, **24**, 89–104, doi:10.1007/s00382-004-0478-x.
- Dekens, P. S., A. C. Ravelo, M. D. McCarthy, and C. A. Edwards, 2008: A 5 million year comparison of Mg/Ca and alkenone paleothermometers. *Geochem. Geophys. Geosyst.*, **9**, Q10001, doi:10.1029/2007GC001931.
- Dijkstra, H., and J. Neelin, 1995: Ocean–atmosphere interaction and the tropical climatology. Part II: Why the Pacific cold tongue is in the east. *J. Climate*, **8**, 1343–1359, doi:10.1175/1520-0442(1995)008<1343:OAIATT>2.0.CO;2.
- DiNezio, P., A. Clement, G. Vecchi, B. Soden, B. Kirtman, and S.-K. Lee, 2009: Climate response of the equatorial Pacific to global warming. *J. Climate*, **22**, 4873–4892, doi:10.1175/2009JCLI2982.1.
- Donohoe, A., and D. Battisti, 2012: What determines meridional heat transport in climate models? *J. Climate*, **25**, 3832–3850, doi:10.1175/JCLI-D-11-00257.1.
- Dowsett, H., and Coauthors, 2012: Assessing confidence in Pliocene sea surface temperatures to evaluate predictive models. *Nat. Climate Change*, **2**, 365–371, doi:10.1038/nclimate1455.
- Emanuel, K., J. D. Neelin, and C. Bretherton, 1994: On large-scale circulations in convecting atmospheres. *Quart. J. Roy. Meteor. Soc.*, **120**, 1111–1143, doi:10.1002/qj.49712051902.
- Fedorov, A. V., 2007: Net energy dissipation rates in the tropical ocean and ENSO dynamics. *J. Climate*, **20**, 1108–1117, doi:10.1175/JCLI4024.1.
- , R. Pacanowski, S. Philander, and G. Boccaletti, 2004: The effect of salinity on the wind-driven circulation and the thermal structure of the upper ocean. *J. Phys. Oceanogr.*, **34**, 1949–1966, doi:10.1175/1520-0485(2004)034<1949:TEOSOT>2.0.CO;2.
- , P. S. Dekens, M. McCarthy, A. C. Ravelo, P. B. deMenocal, M. Barreiro, R. C. Pacanowski, and S. G. Philander, 2006: The Pliocene paradox (mechanisms for a permanent El Niño). *Science*, **312**, 1485–1489, doi:10.1126/science.1122666.
- , C. M. Brierley, and K. Emanuel, 2010: Tropical cyclones and permanent El Niño in the early Pliocene epoch. *Nature*, **463**, 1066–1070, doi:10.1038/nature08831.
- , —, K. T. Lawrence, Z. Liu, P. S. Dekens, and A. Ravelo, 2013: Patterns and mechanisms of early Pliocene warmth. *Nature*, **496**, 43–49, doi:10.1038/nature12003.
- Gent, P., and Coauthors, 2011: The Community Climate System Model version 4. *J. Climate*, **24**, 4973–4991, doi:10.1175/2011JCLI4083.1.
- Gu, D., and S. Philander, 1997: Interdecadal climate fluctuations that depend on exchanges between the tropics and extratropics. *Science*, **275**, 805–807, doi:10.1126/science.275.5301.805.
- Hartmann, D. L., 1994: *Global Physical Climatology*. International Geophysics Series, Vol. 56, Academic Press, 411 pp.
- , and K. Larson, 2002: An important constraint on tropical cloud–climate feedback. *Geophys. Res. Lett.*, **29**, 1951, doi:10.1029/2002GL015835.
- , M. Ockert-Bell, and M. Michelsen, 1992: The effect of cloud type on Earth’s energy balance: Global analysis. *J. Climate*, **5**, 1281–1304, doi:10.1175/1520-0442(1992)005<1281:TEOCTO>2.0.CO;2.
- Haywood, A., P. Valdes, and V. Peck, 2007: A permanent El Niño-like state during the Pliocene? *Paleoceanography*, **22**, PA1213, doi:10.1029/2006PA001323.
- Held, I. M., 2001: The partitioning of the poleward energy transport between the tropical ocean and atmosphere. *J. Atmos. Sci.*, **58**, 943–948, doi:10.1175/1520-0469(2001)058<0943:TPOTPE>2.0.CO;2.
- , and M. J. Suarez, 1974: Simple albedo feedback models of the icecaps. *Tellus*, **26**, 613–629, doi:10.1111/j.2153-3490.1974.tb01641.x.
- , and K. Shell, 2012: Using relative humidity as a state variable in climate feedback analysis. *J. Climate*, **25**, 2578–2582, doi:10.1175/JCLI-D-11-00721.1.
- Kiehl, J., 1994: On the observed near cancellation between longwave and shortwave cloud forcing in tropical regions. *J. Climate*, **7**, 559–565, doi:10.1175/1520-0442(1994)007<0559:OTONCB>2.0.CO;2.
- , and C. Shields, 2014: Sensitivity of the Paleocene–Eocene thermal maximum climate to cloud properties. *Philos. Trans. Roy. Soc. London*, **A371**, doi:10.1098/rsta.2013.0093.

- Knutson, T., and S. Manabe, 1995: Time-mean response over the tropical Pacific to increased CO₂ in a coupled ocean-atmosphere model. *J. Climate*, **8**, 2181–2199, doi:10.1175/1520-0442(1995)008<2181:TMROTT>2.0.CO;2.
- Koutavas, A., P. B. deMenocal, G. Olive, and J. Lynch-Stieglitz, 2006: Mid-Holocene El Niño–Southern Oscillation (ENSO) attenuation revealed by individual foraminifera in eastern tropical Pacific sediments. *Geology*, **34**, 993–996, doi:10.1130/G22810A.1.
- Kump, L., and D. Pollard, 2008: Amplification of Cretaceous warmth by biological cloud feedbacks. *Science*, **320**, 195–195, doi:10.1126/science.1153883.
- Lee, S.-Y., and C. Poulsen, 2005: Tropical Pacific climate response to obliquity forcing in the Pleistocene. *Paleoceanography*, **20**, PA4010, doi:10.1029/2005PA001161.
- Liang, J., X.-Q. Yang, and D.-Z. Sun, 2012: The effect of ENSO events on the tropical Pacific mean climate: Insights from an analytical model. *J. Climate*, **25**, 7590–7606, doi:10.1175/JCLI-D-11-00490.1.
- Liu, Z., and B. Huang, 1997: A coupled theory of tropical climatology: Warm pool, cold tongue, and Walker circulation. *J. Climate*, **10**, 1662–1679, doi:10.1175/1520-0442(1997)010<1662:ACTOTC>2.0.CO;2.
- , and T. Herbert, 2004: High-latitude influence on the eastern equatorial Pacific climate in the early Pleistocene epoch. *Nature*, **427**, 720–723, doi:10.1038/nature02338.
- Lloyd, J., E. Guilyardi, and H. Weller, 2012: The role of atmosphere feedbacks during ENSO in the CMIP3 models. Part III: The shortwave flux feedback. *J. Climate*, **25**, 4275–4293, doi:10.1175/JCLI-D-11-00178.1.
- Locarnini, R. A., A. V. Mishonov, J. I. Antonov, T. P. Boyer, H. E. Garcia, O. K. Baranova, M. M. Zweng, and D. R. Johnson, 2010: *Temperature*. Vol. 1, *World Ocean Atlas 2009*, NOAA Atlas NESDIS 68, 184 pp.
- Loeb, N., B. Wielicki, D. Doelling, G. Smith, D. Keyes, S. Kato, N. Manalo-Smith, and T. Wong, 2009: Toward optimal closure of the earth's top-of-atmosphere radiation budget. *J. Climate*, **22**, 748–766, doi:10.1175/2008JCLI2637.1.
- Lunt, D., A. Haywood, G. Schmidt, U. Salzmann, P. Valdes, and H. Dowsett, 2010: Earth system sensitivity inferred from Pliocene modelling and data. *Nat. Geosci.*, **3**, 60–64, doi:10.1038/ngeo706.
- Ma, C., C. R. Mechoso, A. W. Robertson, and A. Arakawa, 1996: Peruvian stratus clouds and the tropical Pacific circulation: A coupled ocean-atmosphere GCM study. *J. Climate*, **9**, 1635–1645, doi:10.1175/1520-0442(1996)009<1635:PSCATT>2.0.CO;2.
- Mantsis, D., A. Clement, A. Broccoli, and M. Erb, 2011: Climate feedbacks in response to changes in obliquity. *J. Climate*, **24**, 2830–2845, doi:10.1175/2010JCLI3986.1.
- McCreary, J. P. J., and P. Lu, 1994: Interaction between the subtropical and the equatorial oceans: The subtropical cell. *J. Phys. Oceanogr.*, **24**, 466–497.
- McWilliams, J., and P. Gent, 1978: A coupled air and sea model for the tropical Pacific. *J. Atmos. Sci.*, **35**, 962–989, doi:10.1175/1520-0469(1978)035<0962:ACAASM>2.0.CO;2.
- Merlis, T., and T. Schneider, 2011: Changes in zonal surface temperature gradients and Walker circulations in a wide range of climates. *J. Climate*, **24**, 4757–4768, doi:10.1175/2011JCLI4042.1.
- Philander, S., and A. Fedorov, 2003: Role of tropics in changing the response to Milankovich forcing some three million years ago. *Paleoceanography*, **18**, 1045, doi:10.1029/2002PA000837.
- Ramanathan, V., and W. Collins, 1991: Thermodynamic regulation of ocean warming by cirrus clouds deduced from observations of the 1987 El Niño. *Nature*, **351**, 27–32, doi:10.1038/351027a0.
- Ravelo, A., P. Dekens, and M. McCarthy, 2006: Evidence for El Niño-like conditions during the Pliocene. *Geol. Soc. Amer. Today*, **16**, 4–11, doi:10.1130/1052-5173(2006)016<4:EFENLC>2.0.CO;2.
- Reynolds, R., N. Rayner, T. Smith, D. Stokes, and W. Wang, 2002: An improved in situ and satellite SST analysis for climate. *J. Climate*, **15**, 1609–1625, doi:10.1175/1520-0442(2002)015<1609:AISAS>2.0.CO;2.
- Rose, B. E. J., and J. Marshall, 2009: Ocean heat transport, sea ice, and multiple climate states: Insights from energy balance models. *J. Atmos. Sci.*, **66**, 2828–2843, doi:10.1175/2009JAS3039.1.
- Shields, C., D. Bailey, G. Danabasoglu, M. Jochum, J. Kiehl, S. Levis, and S. Park, 2012: The low-resolution CCSM4. *J. Climate*, **25**, 3993–4014, doi:10.1175/JCLI-D-11-00260.1.
- Stephens, G. L., 2005: Cloud feedbacks in the climate system: A critical review. *J. Climate*, **18**, 237–273, doi:10.1175/JCLI-3243.1.
- , and T. J. Greenwald, 1991: The earth's radiation budget and its relation to atmospheric hydrology: 2. Observations of cloud effects. *J. Geophys. Res.*, **96**, 15 325–15 340, doi:10.1029/91JD00972.
- Sun, D.-Z., and Z. Liu, 1996: Dynamic ocean-atmosphere coupling: A thermostat for the tropics. *Science*, **272**, 1148–1150, doi:10.1126/science.272.5265.1148.
- , and T. Zhang, 2006: A regulatory effect of ENSO on the time-mean thermal stratification of the equatorial upper ocean. *Geophys. Res. Lett.*, **33**, L07710, doi:10.1029/2005GL025296.
- Taylor, K., R. Stouffer, and G. Meehl, 2012: An overview of CMIP5 and the experiment design. *Bull. Amer. Meteor. Soc.*, **93**, 485–498, doi:10.1175/BAMS-D-11-00094.1.
- Wang, W., and M. J. McPhaden, 1999: The surface-layer heat balance in the equatorial Pacific Ocean. Part I: Mean seasonal cycle. *J. Phys. Oceanogr.*, **29**, 1812–1831, doi:10.1175/1520-0485(1999)029<1812:TSLHBI>2.0.CO;2.
- Wara, M. W., A. C. Ravelo, and M. L. Delaney, 2005: Permanent El Niño-like conditions during the Pliocene warm period. *Science*, **309**, 758–761, doi:10.1126/science.1112596.
- Wielicki, B., B. Barkstrom, E. Harrison, R. B. Lee III, G. L. Smith, and J. Cooper, 1996: Clouds and the Earth's Radiant Energy System (CERES): An earth observing system experiment. *Bull. Amer. Meteor. Soc.*, **77**, 853–868, doi:10.1175/1520-0477(1996)077<0853:CATERE>2.0.CO;2.
- , and Coauthors, 2002: Evidence for large decadal variability in the tropical mean radiative energy budget. *Science*, **295**, 841–844, doi:10.1126/science.1065837.